Journal of Asian Earth Sciences 173 (2019) 204–224

Contents lists available at ScienceDirect

Journal of Asian Earth Sciences

journal homepage: www.elsevier.com/locate/jseaes

Full length article

# The Cenozoic tectonic evolution of the faulted basins in the northern margin of the Eastern Qinling Mountains, Central China: Constraints from fault kinematic analysis

Wei Shi*, Long Chen, Xingqiang Chen, Min Cen, Yu Zhang

*Institute of Geomechanics, Chinese Academy of Geological Sciences, Beijing 100081, China*
*Key Laboratory of Neotectonic Movement & Geohazard, Ministry of Natural Resources, Beijing 100081, China*

ARTICLE INFO

*Keywords:*
North China Plate
Ordos block
Qinling orogen
Faulted basin
Cenozoic
Fault kinematics

ABSTRACT

A series of NE and NW-trending Cenozoic faulted basins, located at the north margin of the Eastern Qinling Mountains, document Cenozoic intracontinental extension process in Central China. Based on fault kinematic analysis of the faulted basins, coupling with the stratigraphic sequence, we rebuilt a tectonic stress sequence of the faulted basins since the Cenozoic era. Combined with the previous chronological data, we define the Cenozoic faulted basin formation process including two stages of tectonic evolution. The first stage largely presents the NW-SE extensional rifting in a long period from the Paleocene to the Middle-Late Miocene due to northwestward subduction of the Pacific plate. It is marked by the basin occurrence along the north margin of the Eastern Qinling Mountains (e.g., the Sanmenxia, Lushi, Shangluo, and Weihe Basins) in the Paleocene to the Early-Middle Miocene in accordance with a NW-SE extension, and regional basin inversion in the Middle Miocene as the result of a NW-SE compression. The second stage is featured by the three-episode extension since the Middle-Late Miocene, which is probably affected by the combination of the northeastward growth of the Tibetan Plateau and the northwestward subduction of the Pacific Plate. The earliest episode of NW-SE extension caused by regional NE-SW compression in the Late Miocene to Early Pleistocene, which leads to the formation of the Yuncheng Basin. A gentle NE-SW extension subsequently dominated here in the Late Pleistocene, as represented by the widespread appearance of paleo-lakes in the basins. Then the youngest tectonic regime controlled this region, characteristic of a tectonic transpression (ENE-SWS compression and NNW-SSE extension), causing evidently strike-slip activities on the primary faults in the basins.

## 1. Introduction

The North China Plate (NCP) underwent multi-phase intensive intracontinental rifting in the Cenozoic, marked by wide occurrence of faulted basin (Fig. 1; RGAFSO, 1988; Zhang et al., 2003; Yin, 2010; Li et al., 2013). Previous work shows the Cenozoic faulted basins developed at the intersection of the Taihang Mountains (Mts.). belt and Qinling orogen (Fig. 2), which documents the deformation process in the Cenozoic in the intersection of the structural belts (RGAFSO, 1988; Li et al., 2015; Shi et al., 2015).

However, the formation process of the faulted basins and their driving origin have been on a long-term argument, primarily in virtue of the location of the NCP in a combinational effect of the India-Eurasia collision and Pacific-Eurasia convergence (e.g., Molnar and Tapponnier, 1975; Jolivet et al., 1990; Zhang et al., 1998; Tapponnier et al., 2001; Ren et al., 2002; Schellart and Lister, 2005; Yin et al., 2011; Shi et al., 2015a; Zhao et al., 2016; Chen et al., 2018). The sedimentary sequence and paleomagnetic analysis show four stages of sedimentary evolution processes dominate in the Yuncheng Basin since the late Cenozoic (Li et al., 1994; Wang et al., 1996), including regional uplift and distinct subsiding in the Late Miocene to Pliocene, the occurrence of the Yuncheng paleo-lake in the Early Pleistocene, early expansion and later shrink of the paleo-lake in the Middle Pleistocene, and further shrink of the paleo-lake to the Zhongtiao Mt. piedmont since the Late Pleistocene. Evidently, it is difficult to directly connect the tectonic process. The sedimentary analysis of the Weihe Basin defines three stages of deformation processes, involving “passive” rifting in the Middle-Late Eocene to the Late Miocene (7.3 Ma), strike-slip extension during the Late Miocene to the early Quaternary (7.3 Ma-1.2 Ma), and basin inversion and uplift since the early Quaternary (1.2 Ma–present) (Liu and Xue, 2004; Wang et al., 2013). However, it is only presented by the analysis of the Cenozoic strata sequences and deposit environments,

* Corresponding author.

https://doi.org/10.1016/j.jseaes.2019.01.018
Received 9 July 2018; Received in revised form 23 December 2018; Accepted 12 January 2019
Available online 25 January 2019

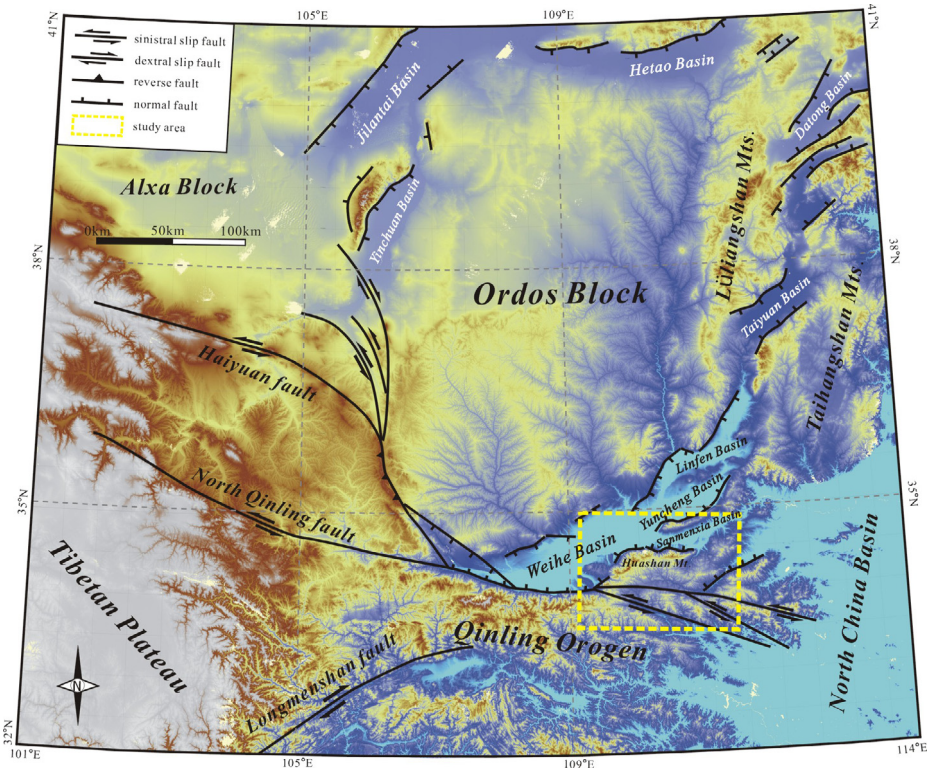


**Fig. 1.** GTOPO30 topographic image showing the structural outline of the central North China and study area.

leading to be difficult to understand the evolution mechanism. The Cenozoic depositional sequence and geophysical comprehensive exploration from the Shanxi Basin reveal that the Yuncheng Basin formed in the Pliocene-Quaternary in virtue of NNW-SSE extension (Xu et al., 1992, 1993). However, the paleomagnetic geochronology of the terraces of the Weihe Basin to the northern margin of the Qinling Mts. shows that NW-SE extension occurred in the area since 2.6 Ma (Sun and Xu, 2007). The fault kinematic analysis in the Weihe Basin shows that the Weihe Basin has undergone a three-stage tectonic evolution since the Cenozoic, the WNW-ESE extension in the Middle-Late Eocene-Early Oligocene linked with the back-arc spreading of the Pacific Plate and the development of the Weihe Basin, the NE-SW extension in the Middle-Late Miocene and accelerating sedimentation and wide subsiding, and the NW-SE extension in the Late Pliocene-Quaternary (Bellier et al., 1988). Based on SPOT (Systeme Probatoire d'Observation de la Terre) remote sensing interpretation, regional structural analysis, and stress field reversion, Zhang et al. (1998, 2006) also proposed a three-stage extension dominated the North China Plate, including this region, leading to the faulted basin formation and corresponding with the counterclockwise rotation of the Ordos block. i.e., NW-SE extension in the early Tertiary and the initiation of the Weihe Basin, NE-SW or NNE-SSW extension in the Miocene and the formation of the Yuncheng and Linfen Basins, NW-SE extension since the Late Pleistocene and continued subsiding of the basins. Mercier et al. (2013) also proposed a four-stage tectonic evolution based on fault kinematic analysis, the NE-SW extension in the Middle Eocene-Early Oligocene and the basin subsiding; the WNW-ESE compression in the Early Oligocene-Early Miocene and faulted basin inversion, NE-SW extension in the Late Miocene-Early Pliocene and basin subsiding, and NW-SE extension in the Late Pliocene to Quaternary and the strike-slip activation. The recent detailed fault kinematic analysis of the boundary faults outlines a three-stage extensive stress fields in this region since the late Cenozoic and basin formation during the Late Miocene to early Quaternary due to NW-SE extension, which is connected with the northeastward grown of the Tibetan Plateau (Shi et al., 2015a). The work shows identical tectonic processes in the Cenozoic due to the detailed chronological data.

Here, our work focuses on the Cenozoic NE- and SE- striking faulted basins at the junction of the Taihangshan tectonic belt and the Qinling orogenic belt. On the basis of fault kinematic analysis of the boundary faults, we rebuild the Cenozoic tectonic process of the faulted basins, linked with their different dynamic background.

## 2. Geological background

The intersection of the Taihang Mts. belt and Qinling orogen is marked by two sets of faults (e.g., NE-striking Huashan Piedmont Fault (HPF) and Zhongtiaoshan Piedmont Fault (ZPF), NW-trending Luonan-Luanchuan Fault and Shang-Dan Fault), and two groups of the Cenozoic faulted basins limited by the two sets of the faults (e.g., Weihe, Sanmenxia, Yuncheng, Lushi, and Luonan Basins) (Fig. 2).

### 2.1. Weihe Basin

The Weihe Basin is located between the Ordos block and the Qinling orogenic belt, and connects with the Sanmenxia and Yuncheng Basins to the west. It has a length of 400 km and a width of 30–80 km (Fig. 2). The basin is marked by half-graben with the maximum Cenozoic sedimentary thickness of 7000 m, as reveled by geophysical data (Ren et al., 2012).

The Cenozoic sedimentary rocks in the Weihe Basin can be divided into nine lithostratigraphic units according to their depositional facies, paleontology and paleomagnetic data (from bottom to top), i.e., the Honghe, Bailuyuan, Lengshuigou, the Koujiacun and Bahe, the Middle-Upper Pleistocene Lantian, the Lower Pleistocene Sanmen, the Middle Pleistocene Tongxiehe, and the Holocene Fms. (Fig. 3; Wang, 1965; BGMSNX, 1989; Li et al., 2016).

The Honghe Fm., overlying on the pre-Sinian rocks with angular unconformity in the basin, is marked by fluvio-lacustrine deposits with purple to red mudstones interbedded with yellow and greyish green

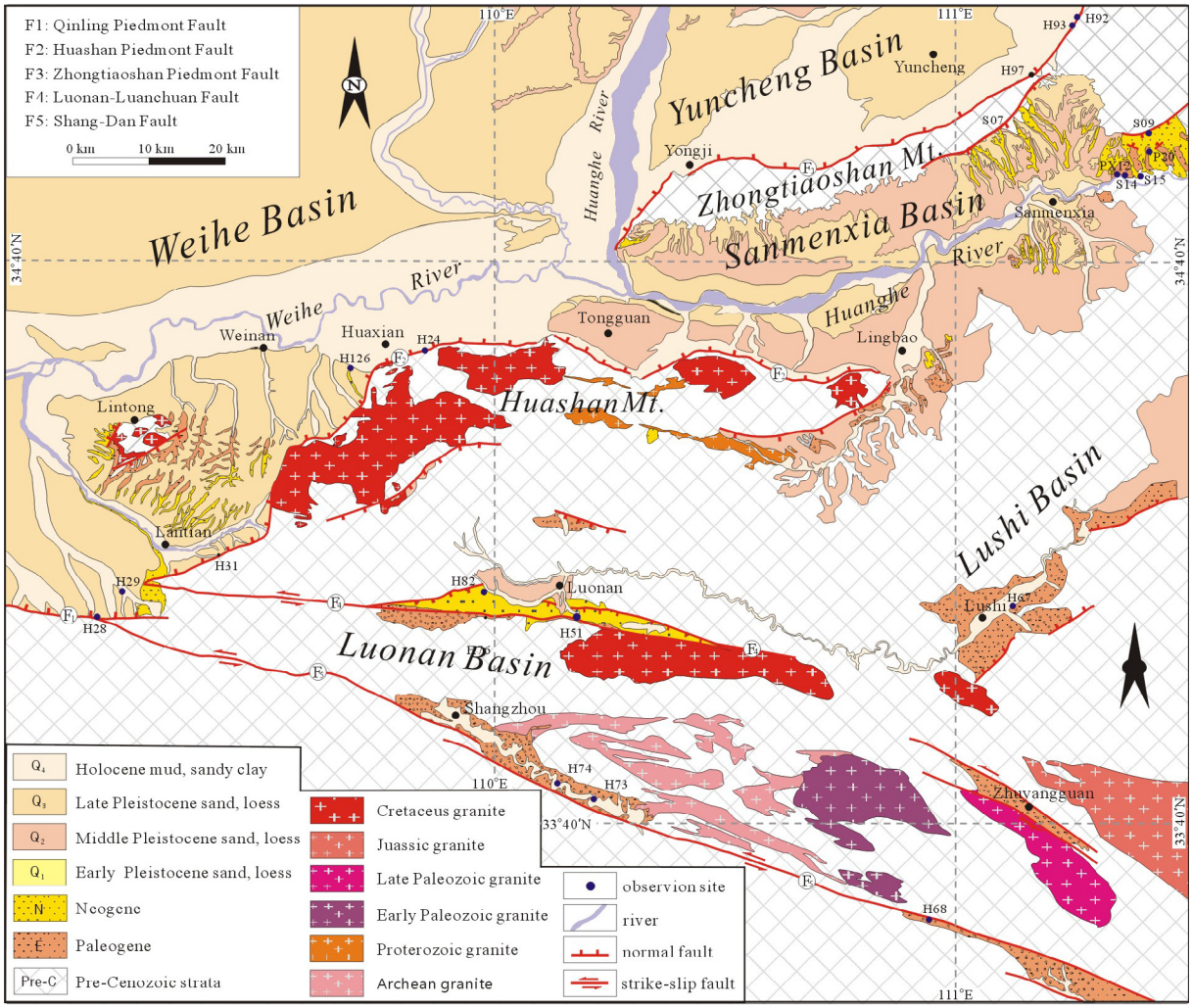


**Fig. 2.** Sketch geological map of the north periphery of the Eastern Qinling Mountains illustrating the structure of the faulted basins.

sandstones and conglomerates at the bottom (Zhang et al., 1978). The fossil vertebrates suggest that the Honghe Fm. was deposited in the Eocene (Liu and Xue, 2004). The Bailuyuan Fm. consists of a series of thick fluvio-lacustrine sediments marked by greyish white medium- to coarse-grained sandstones with intervals of purplish-red mudstones. This formation generally unconformably contacts with the underlying Honghe Fm., and was deposited in the Eocene-Oligocene, as determined from vertebrate and mammals fossils (Zhang et al., 1978; Liu and Xue, 2004). The Lengshuigou Fm. is dominated by yellowish-brown, brownish-red sandstones, interbedded with purple-red mudstone, in angular unconformity contact with the underlying Bailuyuan Fm. (BGMRSNX, 1990). The vertebrate and mammals fossils indicate that this formation is likely the late Early Miocene in age (Liu and Xue, 2004). The Koujiacun Fm. is characteristic of interbedded yellowish brown mudstone and sandstone, and is conformably in contact with the underlying Lengshuigou Fm. The animal and plant fossils indicate that the formation is the Middle Miocene in age (Zhang et al., 1978). The Bahe Fm. is mainly composed of lacustrine deposits marked by interbedded light purple- brown to light yellow mudstone and sandy mudstone, with interval of thin-bedding gray-green mudstone, which is in conformity contact with the underlying Miocene strata. Based on paleomagnetic dating and biostratigraphy, this formation has been interpreted to be Late Miocene with an age of 11–7 Ma (Wang et al., 2013; Kaakinen and Lunkka, 2003). The Lantian Formation is dominated by purplish red clay rocks of lacustrine-fluvial facies. It is rich in spongy calcareous nodules and conglomerate at the bottom, and is in unconformable contact with the underlying Bahe Fm. Based on animal fossils and paleomagnetic testing, the age of the Lantian Fm. is 7.0–2.6 Ma (An et al., 2000). The Upper Pleistocene Sanmen Formation mainly consists of yellow-brown sandy clay with interval of sand and calcium-bearing clay beds, and a gravel bed at the bottom, and with rich in mammalian fossils. The age of the formation covers the interval of 2.5–1.2 Ma, as demonstrated by the new paleomagnetic data from the Songjiabeigou section (Yue et al., 2004), in accordance with the Early Pleistocene. The Middle Pleistocene Xiehu Fm. consists of light grayish-brown, unconsolidated loess interbedded with multiple layers of reddish-brown paleosoil, and the age is coinciding with that of the "Lishi loess" (Liu and Xue, 2004). The Upper Pleistocene Qianxian Fm. is featured by light yellow, loose loess bearing calcareous nodules and 1 or 2 layers of paleosoil, with large pores and vertical joints, in accordance with "Malan loess" (Han et al., 1991). The Holocene is marked by alluvial, pluvial and piedmont alluvial sediments (BGMRHN, 1989).

### 2.2. Sanmenxia Basin

The Sanmenxia Basin, situated between Zhongtiao and Hua Mts., is a NE-striking faulted basin. The basin was filled by relatively complete Cenozoic stratum, from bottom to top, e.g., the Paleogene Mengli, Podi, Xiao'an, and Liulinhe Fms., and Neogene Baode and Jingle Fms., and local Sanmen Fm. (Fig. 3; BGMSNX, 1989; Yue et al., 2004).

The Mengli Fm. is characterized by alluvial fan deposits consisting of gray-brown, dark-purple conglomerate sandwiched sandy mudstone

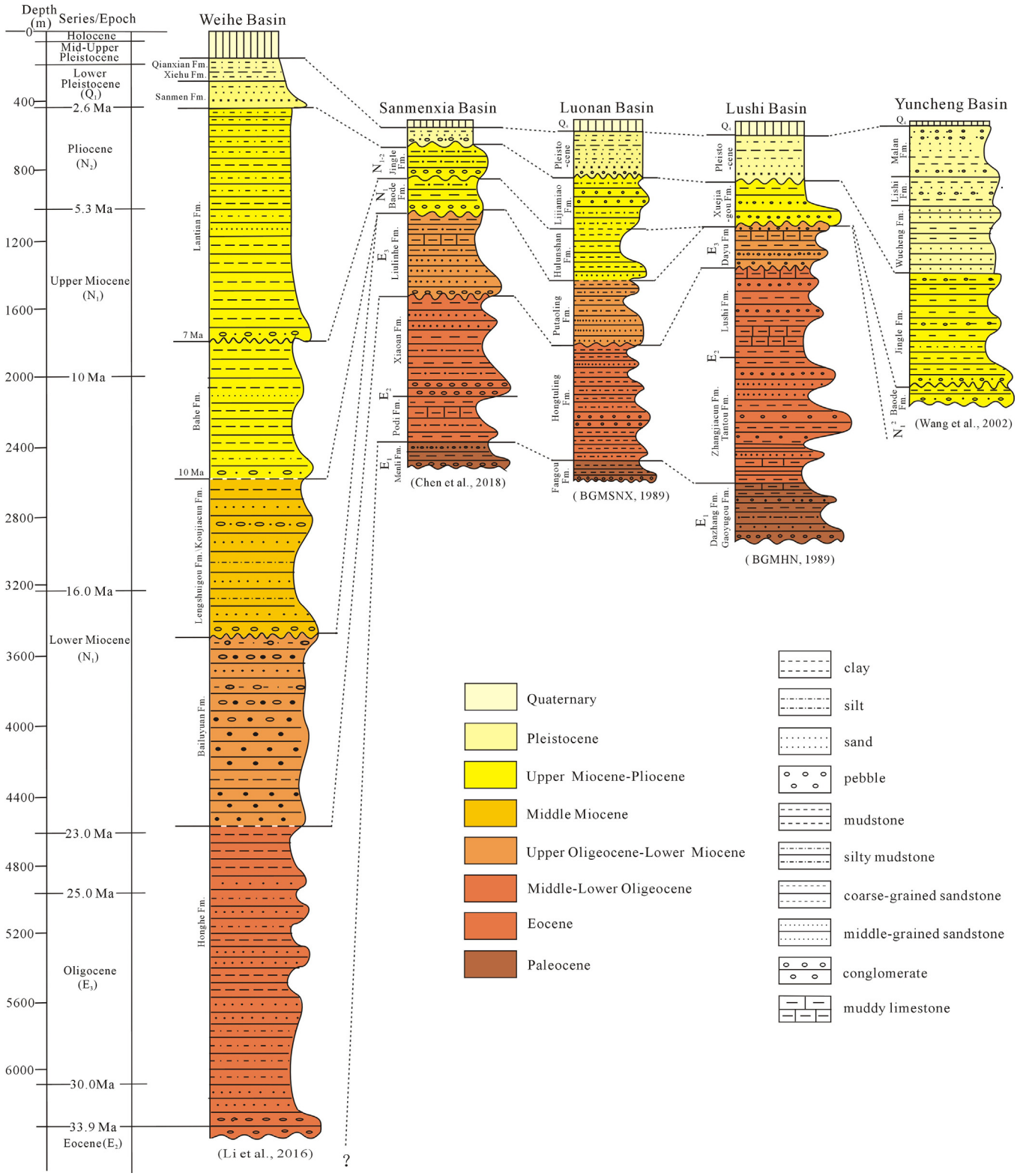


**Fig. 3.** Stratigraphic frameworks of the faulted basins in the north periphery of the Eastern Qinling and the lithostratigraphic correlation.

lenses, with a small amount of clastic limestone. The combination of vertebrate fossils and paleomagnetic data suggests Mengli Fm. sediments were laid down over a period of ca. 54–53 Ma, corresponding to Late Paleocene-Late Eocene (Chen et al., 2018). The Podi Formation is composed of red-brown glutenite sandwiched red sandy mudstone, which turns upwards into red mudstone. It contains ash-green calcareous medium-coarse grained sandstone with a thin layer of oil shale at the top, a sandwiched thin layer of gypsum and limestone, and is a deep lake-delta deposition. Mammalian fossil data indicated that its age is in the Late-Middle Eocene. Magnetic stratigraphy studies further confirmed that the Podi Fm. age ranges from 53 to 42.5 Ma (Tong et al., 2005; Chen et al., 2018). The Xiao'an Fm. consists of fluvial-alluvial red calcareous mudstone sandwiched with thin greyish white, grayish green calcareous sandstones in the lower part, and shallow-deep

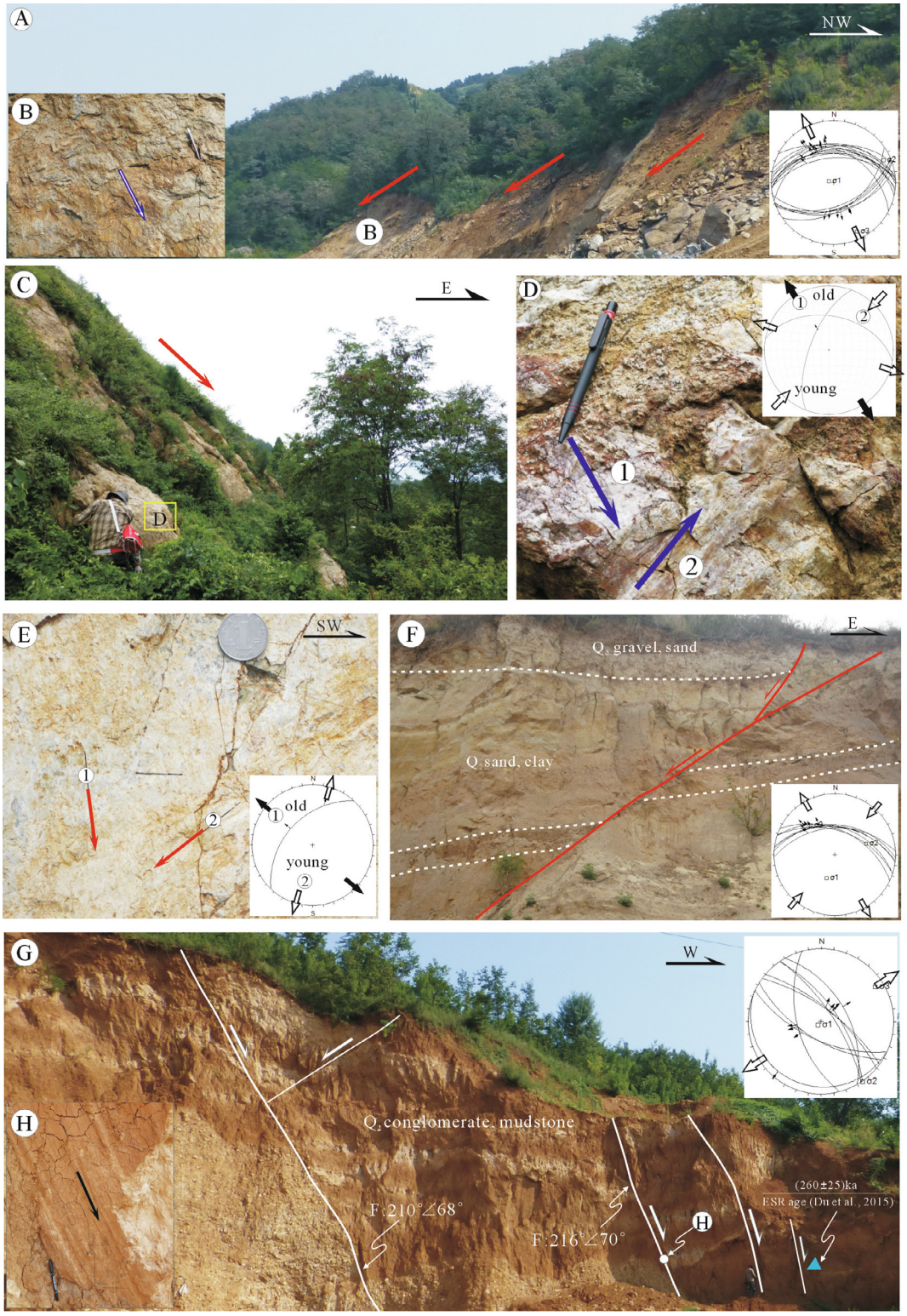


**Fig. 4.** Field photographs shows structural features and deformation in the south margin of the Weihe Basin. (A) Fault facets along the Qinling Piedmont Fault ($F_1$) to the south of the Weihe Basin, and (B) Dip-slip striations on fault facet at the Loc. H28, indicating NW-SE extension. (C) The Huashan Piedmont Fault ($F_2$), typical of fault scarps, documents two stages of activity, early NW-SE extension and NE-SW compression, resulted from dip-slip normal striations and sub-horizontal strike-slip striations, respectively (D). (E) Two groups of the superposed striations developed on the fault plane at the H24, showing early NW-SE extension and later nearly N-S extension. (F) Normal faults in the Middle-Late Pleistocene sand and clay along the Huashan Piedmont Fault (Site H126, the location in Fig. 8) recording NNW-SSE extension and ENE-WSW compression. (G) Normal faults in the Middle Pleistocene sandstone and conglomerate at Site H29 was dominated by NE-SW extension, as calculated by fault kinematic analysis.

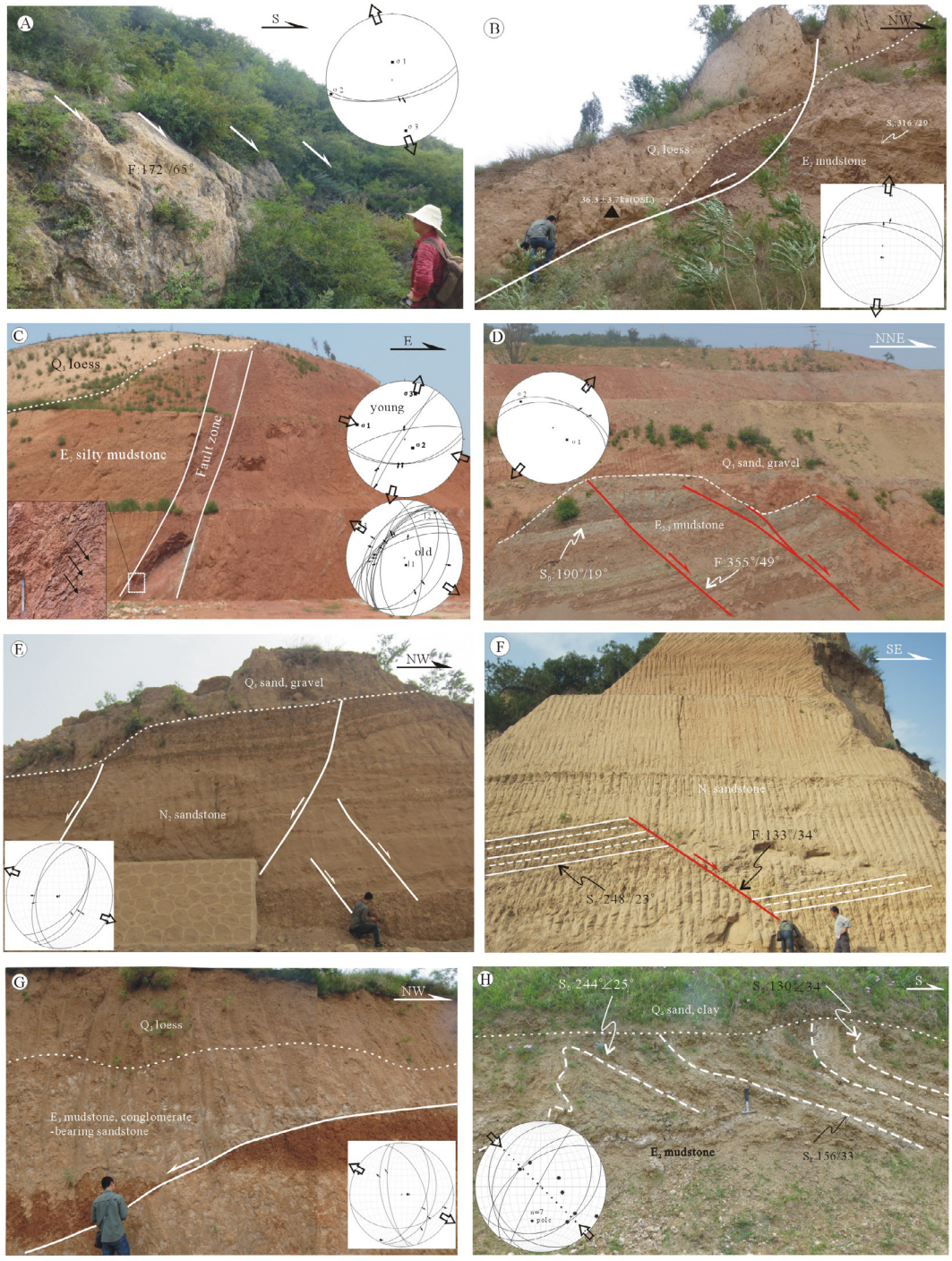


**Fig. 5.** Structural analysis of the eastern Sanmenxia Basin. (A) Fault facets covering with the Late Pleistocene Losses, mark the north margin of the Sanmenxia Basin, on which the striation show NNW-SSE extension. (B) A normal fault cutting Eocene mudstone and Late Pleistocene loess with the OSL age of 36.3 ka near the Yellow River (Loc. S14), and resulted from N-S striking extension. (C) Fault zone in the Eocene silty mudstone strata marking by the early NW-SE extension and later east-west compression and N-S extension from the fault slip vectors near the Sanmenxia Dam (Loc. PX12). (D) Synsedimentary normal faults in the Late Pleistocene sand and pebble deposit in the eastern Sanmenxia Basin (Loc. P20), largely implying NE-SW extension from the fault slip vectors in the Eocene-Oligocene mudstone. (E) A set of northeast-trending in the Pliocene sandstone and its fault-slip vectors determining NW-SE extension prior to the Holocene due to the covering of the faults by the Holocene sand (Loc. S15). Locally, another set of synsedimentary faults with the striking/dip of 133°∠34° in the thick-bedding Pliocene sandstone, indicating NW-SE extension (F). (G) A normal fault cut the Oligocene red thick-bending mudstone and is covered by the Late Pleistocene losses in the northeast basin (Loc. S07), corresponding with NW-SE extension prior to the Late Pleistocene. (H) Eocene thin-bedding mudstone was intensively contracted with NW-SE trending (Loc. S09). See the locations in Figs. 12 and 13. A hammer (35 cm long) for scale. (For interpretation of the references to colour in this figure legend, the reader is referred to the web version of this article.)

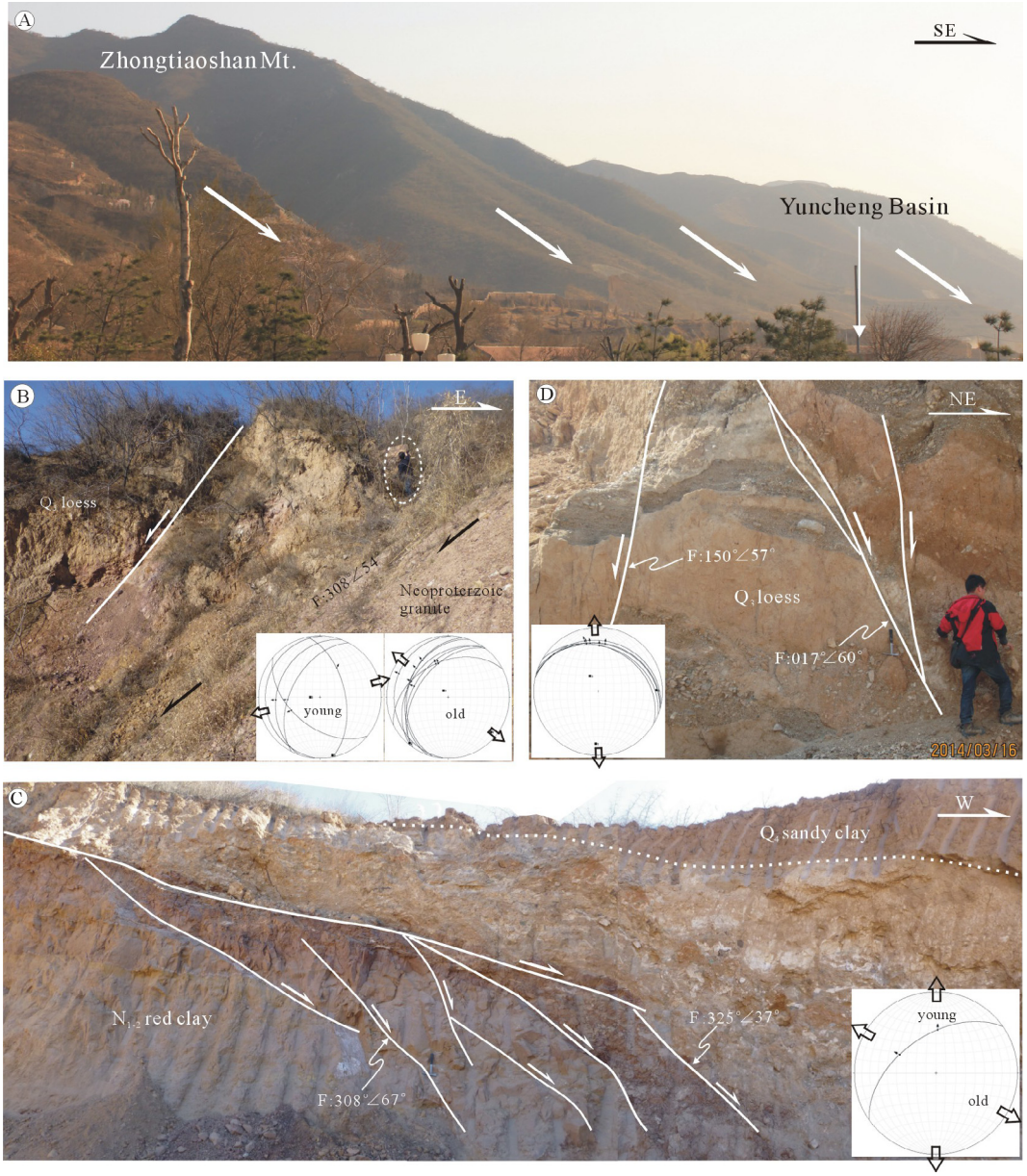


**Fig. 6.** Deformation analysis in the Yuncheng Basin. (A) The Zhongtiaoshan Piedmont Fault to the south side of Yuncheng Basin, typical of fault facets. (B) The Zhongtiaoshan Piedmont Fault is presented by two stages of normal faulting, early NW–SE, and later NE–SW extension resulted from fault slip vectors from main fault and fault in the Late Pleistocene loess, respectively at H92. (C) Two groups of normal faults occurred in the Miocene-Pliocene red thick-bedding mudstone, consistent with early NW–SE extension and later NNW–SSE extension, respectively at H97 (Shi et al., 2015a). (D) A group of high-angle normal faults in the Late Pleistocene strata near the Zhongtiaoshan Piedmont Fault, associated with NNW–SSE extension (H97). A hammer (35 cm long) for scales. (For interpretation of the references to colour in this figure legend, the reader is referred to the web version of this article.)

lacustrine interbedded gray-white calcareous mudstone and red mudstone, with interval of gray-green mudstone, oil shale, and gypsum in the upper part. The paleomagnetic dating coeval with mammalian fossils delimits the age of the formation spans the interval of ca. 42.5–27 Ma, associated with the Eocene–Early Oligocene (Tong et al., 2005; Chen et al., 2018).

The Liulinhe Fm. is composed of red mudstone, calcareous mudstone interbedded with gray sandstone in the lower part, and red calcareous mudstone sandwiched thin gray mudstone and limestone in upper part. A paleomagnetic work determines its age range is 26–12.5 Ma (Chen et al., in review). The Baode Fm. is marked by alluvial fan deposits consisting of thick-bedding conglomerate sandwiched with massive fine-grain sandstone, and deposit in an age range of 11.5–7 Ma, as suggested by new paleomagnetic work (Chen et al., in review). The Jingle Fm. is interbedded brick-red clay and grayish-white calcareous nodules with a local gravel layer. Paleomagnetic analysis showed that the age range of the Jingle Fm. is 6.5–2.6 Ma (Chen et al., in review). The Sanmen Fm. is marked by lacustrine deposits of a yellow-brown sandy clay sandwiched sand beds. A paleomagnetic testing shows that the Sanmen Fm. deposits at ~5 Ma-150 ka (Wang et al., 2004).

### 2.3. Yuncheng Basin

The Yuncheng Basin is a half-graben bounded by the Zhongtiaoshan Fault ($F_3$) to the south, filled by a late Cenozoic deposit (Fig. 3; Wang et al., 2002). The basin is the southernmost basin in the Shanxi Rift with the strikes of the ENE–WSW, ~50 km wide and ~140 km long (Fig. 2), The basin is separated from the Linfeng Basin by the Emei uplift, a Cretaceous granite intrusion with a mean U–Pb age of ca.

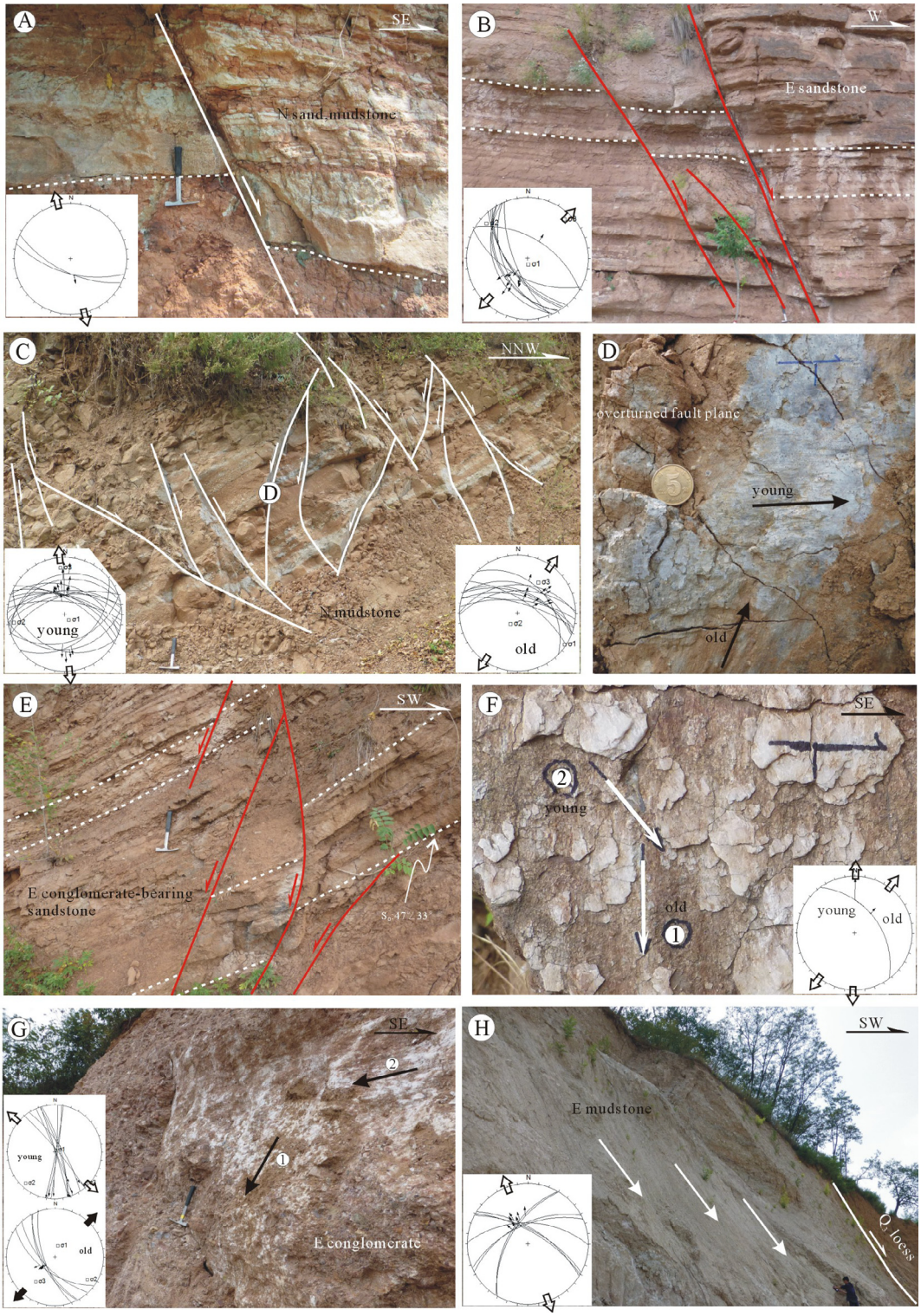


**Fig. 7.** Structural investigation in the Luonan and Lushi basins. (A) A normal fault grown in the Neogene red mudstone interbedded conglomerate with the vertical offset of 30 cm in the interior of the Luonan Basin (Loc. H51), associated with N-S trending extension. (B) A ground of normal faults cutting Paloegene red sandstone with the interval of conglomerate to the south side of the Luonan Basin, characteristic of a NE-SW extension (Loc. H74). (C) Two sets of normal faults in the Neogene red mudstone in the northwest of the Luonan Basin (Loc. H82), showing the early NE-SW extension, and younger N-S extension from the superposed fault slip vectors (D). (E) A set of faults in the Paleogene red medium- to thick-bedding sandstone interbedded conglomerate in the middle segment of the Shang-Dan Fault (Loc. H73), indicating early NE-SW and later N-S extension inferred from their fault kinematic analysis, coeval with their crosscutting relationship (F). (G) Two generations of the striations grow on the fault plane, including dip-slip and oblique-slip striations, respectively showing early NW-SE extension and later NNW-SSE extension in the east segment of the Shang-Dan Fault (Loc. H68). (H) A set of large fault in the Paleogene gray mudstone at Loc. H67 defining NNW-SSE extension. A hammer (35 cm long) for scales. (For interpretation of the references to colour in this figure legend, the reader is referred to the web version of this article.)

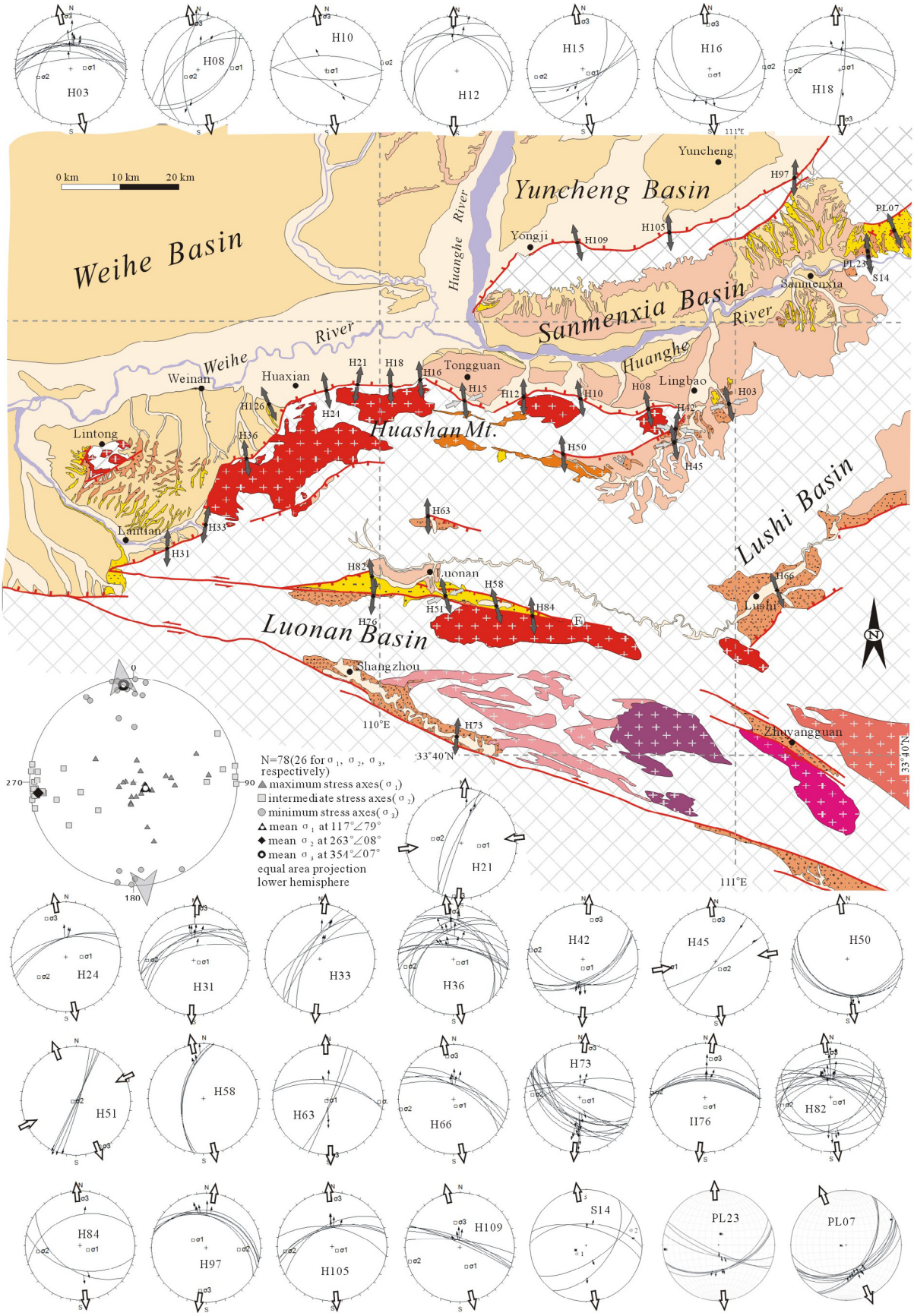


**Fig. 8.** The Late Pleistocene-Holocene NNW-SSE extensional stress field in the north periphery of the Eastern Qinling Mountains, derived from analysis of fault-slip data. Same legends as Fig. 2. Stereonets show principal stress directions (Equal angle projection, lower hemisphere). The numbers 1, 2, and 3 on plots represent minimum, medium, and maximum principal stress, respectively. The opposing gray arrows present the minimum principal stress ($\sigma_3$) direction. Same legends as Fig. 2. The stereograms are derived from analysis of the fault slip vectors by software Faultkin 6 from Dr. Rick Allmendinger.

**Table 1**
A NNW-SSE extensional paleo-stress field in the north periphery of the Eastern Qinling Mountains derived from the fault slip vectors.

| Site | Longitude (E) | Latitude (N) | Stratigraphy-lithology | Vector number | $\sigma_1$ (az°/pl°) | $\sigma_2$ (az°/pl°) | $\sigma_3$ (az°/pl°) |
|---|---|---|---|---|---|---|---|
| H03 | 110°58′08″ | 34°29′30″ | E conglomerate | 9 | 080/64 | 257/25 | 348/01 |
| H08 | 110°33′22″ | 34°29′55″ | granite fault facet | 6 | 085/28 | 259/47 | 358/08 |
| H10 | 110°33′23″ | 34°29′55″ | granite fault facet | 3 | 189/89 | 081/01 | 351/01 |
| H12 | 110°24′09″ | 34°29′50″ | granite fault facet | 4 | 066/34 | 231/54 | 331/07 |
| H15 | 110°14′11″ | 34°29′07″ | gneiss fault facet | 4 | 127/79 | 262/07 | 353/07 |
| H16 | 110°07′09″ | 34°31′59″ | gneiss fault facet | 3 | 187/78 | 087/02 | 356/11 |
| H18 | 110°01′56″ | 34°31′02″ | gneiss fault facet | 4 | 034/80 | 270/05 | 179/07 |
| H21 | 109°56′25″ | 34°30′56″ | gneiss fault facet | 3 | 095/57 | 281/32 | 189/02 |
| H24 | 109°51′18″ | 34°30′25″ | gneiss fault facet | 3 | 084/60 | 236/26 | 332/12 |
| H31 | 109°25′53″ | 34°07′53″ | gneiss fault facet | 7 | 103/81 | 271/08 | 001/01 |
| H33 | 109°32′21″ | 34°10′42″ | gneiss fault facet | 5 | 042/36 | 155/27 | N-S |
| H36 | 109°38′09″ | 34°20′25″ | gneiss fault facet | 15 | 130/80 | 262/06 | 353/06 |
| H42 | 110°49′13″ | 34°26′03″ | gneiss fault facet | 6 | 187/73 | 280/01 | 010/16 |
| H50 | 110°30′57″ | 34°22′14″ | granite fault facet | 5 | 161/39 | 263/14 | 010/46 |
| H63 | 110°08′15″ | 34°13′05″ | E conglomerate | 4 | 271/84 | 091/01 | 181/01 |
| H66 | 111°06′15″ | 34°04′05″ | E conglomerate | 5 | 169/78 | 260/01 | 350/11 |
| H73 | 110°14′04″ | 33°43′06″ | E conglomerate | 15 | 127/80 | 276/08 | 007/04 |
| H76 | 109°59′42″ | 34°01′14″ | E conglomerate fault | 6 | 186/72 | 276/01 | 006/17 |
| H82 | 109°59′32″ | 34°04′57″ | N conglomerate | 16 | 146/79 | 262/04 | 353/09 |
| H84 | 109°59′53″ | 34°03′52″ | E sandstone | 3 | 115/74 | 264/13 | 355/07 |
| H97 | 111°09′00″ | 35°00′32″ | gneiss fault facet | 5 | 301/55 | 090/30 | 189/14 |
| H105 | 110°47′49″ | 34°52′39″ | gneiss fault facet | 5 | 129/80 | 266/06 | 356/06 |
| H109 | 110°32′32″ | 34°51′19″ | gneiss fault facet | 5 | 163/52 | 255/02 | 347/37 |
| PL 07 | 111°25′29″ | 34°53′29″ | $E_{2-3}$ mudstone | 10 | 266/82 | 060/07 | 151/04 |
| PL23 | 111°22′28″ | 34°50′57″ | $E_{1-2}$ conglomerate | 7 | 009/73 | 266/04 | 175/16 |
| S14 | 111°21′48″ | 34°50′15″ | $N_2$ sandstone | 4 | 250/78 | 082/14 | 351/02 |

$\sigma_1$, $\sigma_2$, $\sigma_3$ correspond to maximum, intermediate, and minimum compressive stress, respectively; az°-azimuth, pl°-plunge, $R=(\sigma_2-\sigma_3/\sigma_1-\sigma_3)$; E-Paleocene, $E_{2-3}$-Eocene-Oligocene, $E_3$-$N_1$-Oligocene-Miocene, N-Neocene, $N_1$-Miocene.

132 ± 9.2 Ma (Qi et al., 2011).

The late Cenozoic sedimentary rocks in the Yuncheng Basin are divided into the following five lithostratigraphic units according to depositional facies, paleontology, and paleomagnetic data (from bottom to top): (1) the Late Miocene–Pliocene Kouzhai Fm.; (2) the Pliocene Nanyulin Fm.; (3) the Early–Middle Pleistocene Nihewan Fm.; (4) the Late Pleistocene Malan Fm.; and (5) Holocene sediments (BGMSX, 1989).

The Kouzhai Fm. (86–236 m thick) is a lacustrine sequence of gray to gray-brown mudstone and silty mudstone, interbedded siltstone and marl, resting on Archean metamorphic basement, Mesozoic limestone (Wang et al., 2002). The Kouzhai Fm. was deposited in the Late Miocene–Pliocene, associated with the Hipparion red clay, which has a paleomagnetic age span of ca. 10–2 Ma (Yue et al., 2004; Li et al., 2013). The Nanyulin Fm. with 63–254 m in thickness conformably overlies the Kouzhai Fm., and is overlain by the Nihewan Fm. The formation consists of lacustrine interbedded gray–green mudstone and coarse sandstone, medium- and fine-grained sandstone, siltstone, and marl, coinciding with Pliocene (GSBSX, 2007). The Nihewan Fm. is characterized by horizontally bedding and cross-stratified fluvio-lacustrine, gray-green siltstone and grayish-yellow sandstone (Min et al., 2006). The mammalian fossils hosted in the rock (e.g., Erinaceus cf. dealbatus, Alactaga cf. annulatus, Nyctereutes sinensis, Palaeoloxodon namadicus; Zhou et al., 1991; Qiu and Qiu, 1995; Qiu, 2000) and magnetostratigraphic data (Min et al., 2006; Zhu et al., 2007; Li et al., 2008) suggest the timing of deposition of the Nihewan Fm. to the Early Pleistocene (2.6–0.11 Ma). The Malan Fm. was deposited in the Late Pleistocene and consists of massive, aeolian yellow sandy clay (Liu, 1985; Lu et al., 1987). The Malan Fm. unconformably overlies a variety of older strata and is widely distributed on hills throughout the basin. Holocene sandy clay predominates along river banks.

### 2.4. Lushi Basin

The Lushi Basin with NE striking, located on the northern margin of the East Qinling Mts., is characteristic of half-graben basin (Figs. 1 and 2). The sedimentary strata of the Lushi Basin from bottom to up are the Paleogene Gaoyugou, Dazhang. Tantou, Zhangjiacun, Lushi, and Dayu Fms., and the Neogene Xuejiagou Fm. with local distribution of the Quaternary strata (BGMRHN, 1990).

The Gaoyugou Fm. is composed of a purplish-red clay rock with a conglomerate in the lower part and greyish green sandstone in the upper part. The animal fossils delimit the age of the formation spans the Early-Middle Paleocene. The Dazhang Fm. is marked by dark red, gray-green claystone and gray-white limestone, interbedded with oil-shale shale in the upper. It is in conformity contact with the underlying Gaoyugou Formation. The animal and plant fossils indicate the formation was formed in the Late Paleocene.

The Tantou Fm. mainly consists of greyish green, greyish white and greyish black claystones, with interval of marl and oil shale. The formation is in conformity contact with the underlying Gaoyugou Formation. The combination of animal and plant fossils determined its sedimentation age of the Early Eocene (BGMRHN, 1990). The Zhangjiacun Fm. is featured by a floodplain deposit of purple-red, brick-red mudstone, sandstone and conglomerate. Sporopollen analysis indicates that it was probably formed in the Middle Eocene (Yang et al., 2005). The Lushi Fm. mainly consists of lacustrine fluvial sedimentary rocks of interbedded muddy dolomite and dolomitic mudstone in the lower part, and interbedded argillaceous limestone and calcareous sandstone. The formation was deposited in Late Eocene, as delimited by the animal fossils and sporopollen assemblage (BGMRHN, 1990; Yang et al., 2005). The Dayu Fm. is characteristic of brown semi-concrete conglomerate and sandy conglomerate, with local inclusions of gray-green claystone and marl. The sporopollen assemblage indicates that it is an Oligocene deposit (Yang et al., 2005). The formation contacts with the underlying Lushi Fm. with angular unconformity.

The Xuejiagou Fm. developed in the Neogene of the Lushi Basin, marked by fluvial-pluvial red conglomerate in the lower part, and red, gray-yellow sandy claystone and fine-grained sandstones with calcareous nodules in the upper part. The formation is angularly unconformable on the Dayu Formation, corresponding with the Early Pliocene inferred from mammalian fossil data. The Quaternary strata mainly consist of the Middle Pleistocene and the Holocene. The Middle Pleistocene is dominated by eolian loess and contains calcareous

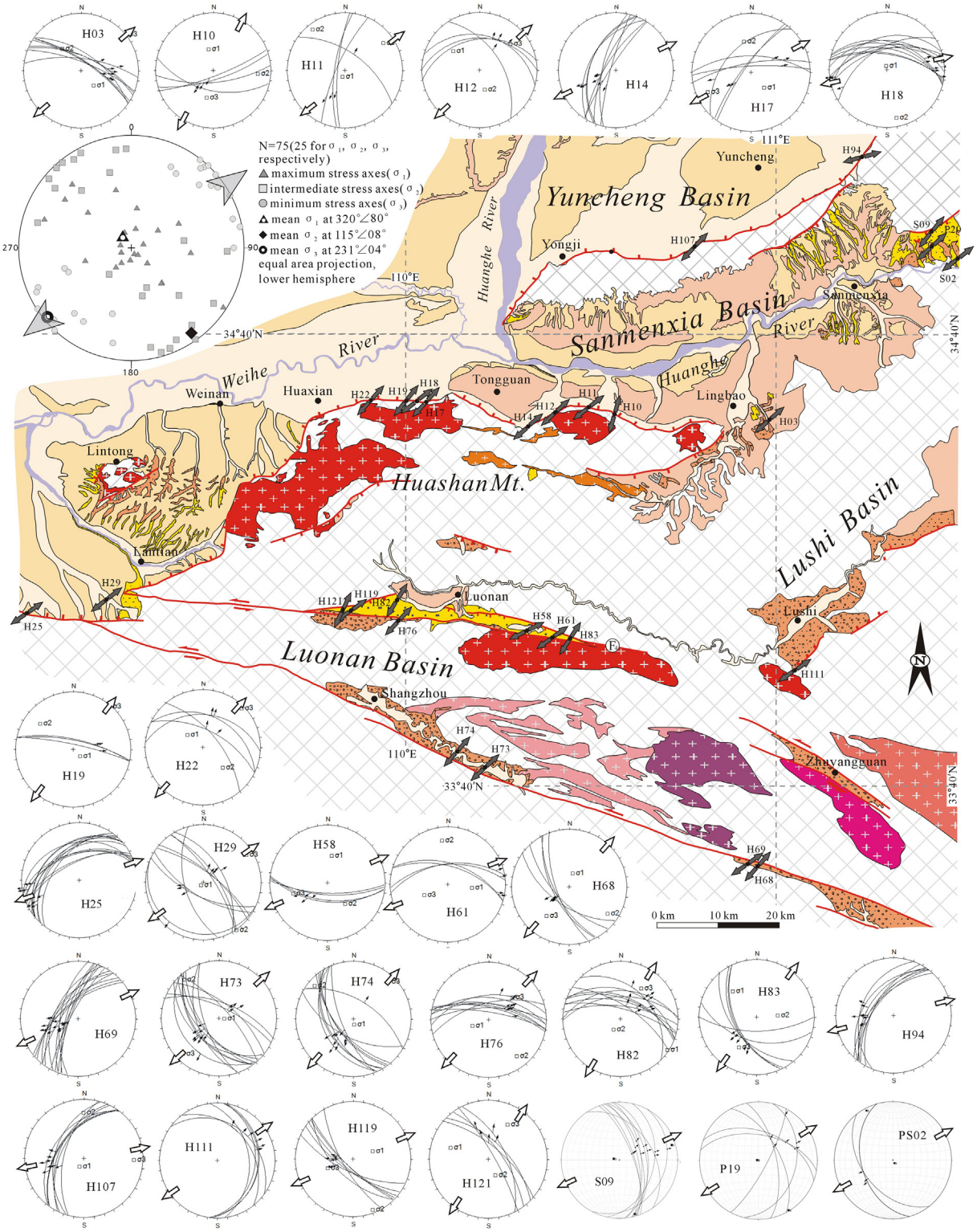


**Fig. 9.** The Late Pleistocene NE-SW extensional paleo-stress field in the north periphery of the Eastern Qinling Mountains, based on the fault kinematic analysis (Equal angle projection, lower hemisphere). Opposing gray arrows present the minimum principal stress ($\sigma_3$) direction. Same legends as Fig. 2. The stereograms are also calculated by software Faultkin 6 from Dr. Rick Allmendinger.

nodules. The Holocene is characteristic of fluvial deposition, which is preliminarily distributed along the river.

### 2.5. Shangluo Basin

Shangluo Basin is a faulted basin in the north of the East Qinling Mts., limited by the NW- to WNW-trending Shang-Dan fault (F4) Luonan-Luanchuan fault ($F_5$) to the south. The Cenozoic sedimentary rocks in the Shangluo Basin can be divided into five lithostratigraphic units according to their depositional facies, paleontology and paleomagnetic data (from bottom to top), i.e., the Paleocene Fangou Fm., Eocene Hongtuling Fm., and Oligocene Putaoling Fm., Miocene

**Table 2**
Results of Fault-slip vector analysis and stress regime in the north periphery of the Eastern Qinling Mountains defining a NE-SW extensional stress regime.

| Site | Longitude (E) | Latitude (N) | Stratigraphy-lithology | Vector number | $\sigma_1$ (az°/pl°) | $\sigma_2$ (az°/pl°) | $\sigma_3$ (az°/pl°) |
|---|---|---|---|---|---|---|---|
| H03 | 110°58′08″ | 34°29′30″ | E conglomerate | 8 | 139/56 | 319/33 | 049/01 |
| H10 | 110°33′23″ | 34°29′55″ | granite fault facet | 4 | 345/46 | 092/16 | 196/39 |
| H11 | 110°29′09″ | 34°30′40″ | marble fault facet | 4 | 213/77 | 321/03 | 052/11 |
| H12 | 110°24′10″ | 34°29′50″ | granite fault facet | 4 | 306/28 | 167/54 | 047/19 |
| H14 | 110°19′17″ | 34°27′49″ | gneiss fault facet | 8 | | | NE-SW |
| H17 | 110°03′25″ | 34°31′09″ | gneiss fault facet | 6 | 140/56 | 344/31 | 247/11 |
| H18 | 110°03′25″ | 34°31′09″ | gneiss fault facet | 11 | 336/78 | 169/11 | 079/02 |
| H19 | 110°00′25″ | 34°31′04″ | gneiss fault facet | 3 | 134/74 | 308/15 | 038/01 |
| H22 | 109°54′38″ | 34°31′13″ | gneiss fault facet | 4 | 309/49 | 135/40 | 042/04 |
| H25 | 109°10′16″ | 34°04′50″ | gneiss fault facet | 13 | | | NE-SW |
| H29 | 109°13′26″ | 34°03′57″ | gneiss fault facet | 10 | 245/82 | 145/01 | 055/07 |
| H58 | 110°20′00″ | 34°01′21″ | $N_1$ conglomerate | 8 | 352/57 | 172/32 | NE-SW |
| H61 | 110°26′03″ | 33°59′59″ | granite fault facet | 4 | 095/46 | 351/13 | 249/40 |
| H68 | 110°57′09″ | 33°30′50″ | E conglomerate | 5 | 008/61 | 124/13 | 221/24 |
| H69 | 110°55′35″ | 33°31′09″ | E conglomerate | 18 | 177/45 | 038/37 | NE-SW |
| H73 | 110°14′04″ | 33°43′06″ | E conglomerate | 13 | 074/81 | 317/03 | 227/07 |
| H74 | 110°09′33″ | 33°45′12″ | E conglomerate | 10 | 185/81 | 310/05 | 041/07 |
| H76 | 109°59′42″ | 34°01′14″ | E conglomerate fault | 9 | 254/55 | 142/14 | 043/00 |
| H82 | 109°59′32″ | 34°04′57″ | N conglomerate | 10 | 123/03 | 220/65 | 031/24 |
| H83 | 109°59′50″ | 34°03′31″ | E conglomerate | 6 | 317/24 | 082/51 | 213/23 |
| H94 | 111°12′13″ | 35°04′05″ | gneiss fault facet | 8 | 013/76 | 154/10 | 245/08 |
| H107 | 110°46′02″ | 34°51′48″ | gneiss fault facet | 8 | 218/72 | 357/13 | 090/10 |
| H111 | 111°02′30″ | 33°56′44″ | E conglomerate | 6 | 057/67 | 285/15 | 191/15 |
| H119 | 109°53′29″ | 34°03′12″ | $N_1$ conglomerate | 7 | 063/51 | 159/05 | 253/38 |
| H121 | 109°53′21″ | 34°03′15″ | E conglomerate | 5 | 288/20 | 159/59 | 026/21 |
| S09 | 111°22′25″ | 34°52′12″ | $E_{2\text{-}3}$ mudstone | 14 | 283/82 | 164/04 | 074/07 |
| PS02 | 111°29′11″ | 34°50′00″ | O limestone | 3 | 155/85 | 332/05 | 062/01 |
| P19 | 111°23′35″ | 34°52′32″ | $E_{2\text{-}3}$ conglomerate | 6 | 137/83 | 327/07 | 237/01 |

$\sigma_1$, $\sigma_2$, $\sigma_3$ correspond to maximum, intermediate, and minimum compressive stress, respectively; az°-azimuth, pl°-plunge, R = ($\sigma_2$-$\sigma_3$/$\sigma_1$-$\sigma_3$); O-Ordovician, E-Paleocene, $E_2$-$_3$-Eocene-Oligocene, $E_3$-$N_1$-Oligocene-Miocene, N-Neocene, $N_1$-Miocene.

Hulunshan Fm. and Pliocene Lijiamiao Fm., and a Lower Pleistocene alluvial-pluvial gravel and Middle Pleistocene lacustrine sandstone, Upper Pleistocene aeolian loess, and the Holocene alluvial and pluvial gravel (Fig. 3; BGMSNX, 1989).

The Fangou Fm. is dominated by lacustrine brown-red, purple-red mudstone, sandy mudstone, and glutenite, and is angularly unconformable on the pre-Cenozoic strata. The Hongtuling Fm. is composed of lacustrine yellow-brown and brown-red sandy mudstones with the interval of conglomerate and sandstone, calcium nodules, which is in conformity contact with the underlying Fangou Formation. The Putaoling Fm. is composed of interbedded white conglomerate, sandstone, yellow-brown mudstone. The contact between the Putaoling and Hongtuling Fms. is generally angularly conformable. The Hulunshan Fm. is a grey glutenite and conglomerate of river alluvial-pluvial facies, which is in parallel unconformity contact with the underlying Putaoling Fm. The Lijiamiao Fm. is composed of fluvial brown-red sandy mudstone with the interval of conglomerate, and is in parallel unconformity contact with the underlying Hulunshan Fm. (Fig. 3).

## 3. Structural investigation and fault kinematics analysis

Our structural investigation focuses on the boundary faults of the Cenozoic basins, which is more propitious to define the basin formation and deformation. Here we orderly decipher structural observation and the fault kinematics analysis on the five basins with a few representative outcrop-scale examples, as exhibited in Figs. 4–7, which delimit the sequence and timing of deformation.

### 3.1. The east margin of the Weihe Basin

The Weihe Basin is bounded by the NE-striking Qinling Piedmont Fault ($F_1$) and NE-striking Huashan Piedmont Fault ($F_2$) to the south, marked by fault facets with a dip angle of 60–70° (Fig. 4A; RGAFSO, 1988; Hou et al., 1995). The Qinling Piedmont Fault was well outcropped at Tangxi Town (Loc. H28, see the location in Fig. 2), with the dip of ~ 30°. A group of normal dip-slip striations grows on the fault plane, which indicates NW-SE extension (Fig. 4B). The Huashan Piedmont Fault extends along the northern margin of Huashan Mt. with the length of ~100 km and the dip of 40–60°. The fault is also characterized by fault facets, as shown in the east of Lantian County (Loc. H31; Fig. 4C), where two sets of striations develop, old normal dip-slip and the later oblique slip, and young oblique-slip striations, showing early NW-SE extensional activity and the later NE-SW compressional activity, respectively (Fig. 4D). The Huashan Piedmont Fault is also well exposed in the east of Hua County (Loc. H24), where the boundary fault is marked by orderly NW-SE and N-S extension, as indicated by the analysis of fault slip vectors from normal dip-slip and oblique-slip striations on the one fault plane, respectively (Fig. 4E). At Site H126 the piedmont of the Huashan Mt., a fault cuts the Middle-Late Pleistocene light yellow sand and red clay; here one set of striations grew on the fault plane, marked by normal dip-slip activity, indicating transtensional stress regime (NNW-SSE extension and ENE-WSW compression). Its activity likely occurred in or posterior to the Late Pleistocene, as inferred by the youngest strata cut by the fault (Fig. 4F). To the south of Lantian County (Loc. H29), a group of normal faults developed in the Middle Pleistocene red mudstone and gray-white conglomerate, generating a most fault offset with ca. 10 m (Fig. 4G). Only one group of dip-slip striations developed on the fault surface (Fig. 4H), showing a NE-SW extensional activity, which occurred after the deposition in the Middle Pleistocene in this area.

As analyzed above, coeval with fault crosscutting relationships, four stages of Cenozoic deformation are defined in the east of the Weihe Basin, and orderly NW-SE extension, NE-SW compression, NE-SW extension, and nearly NNW-SSE extension.

### 3.2. The east margin of the Sanmenxia Basin

The Sanmenxia Basin is bounded by faults to the south and partly by faults to north. A boundary fault is exposed in the north of Sanmenxia, with the footwall consisting of Archaeozoic marble and the hanging

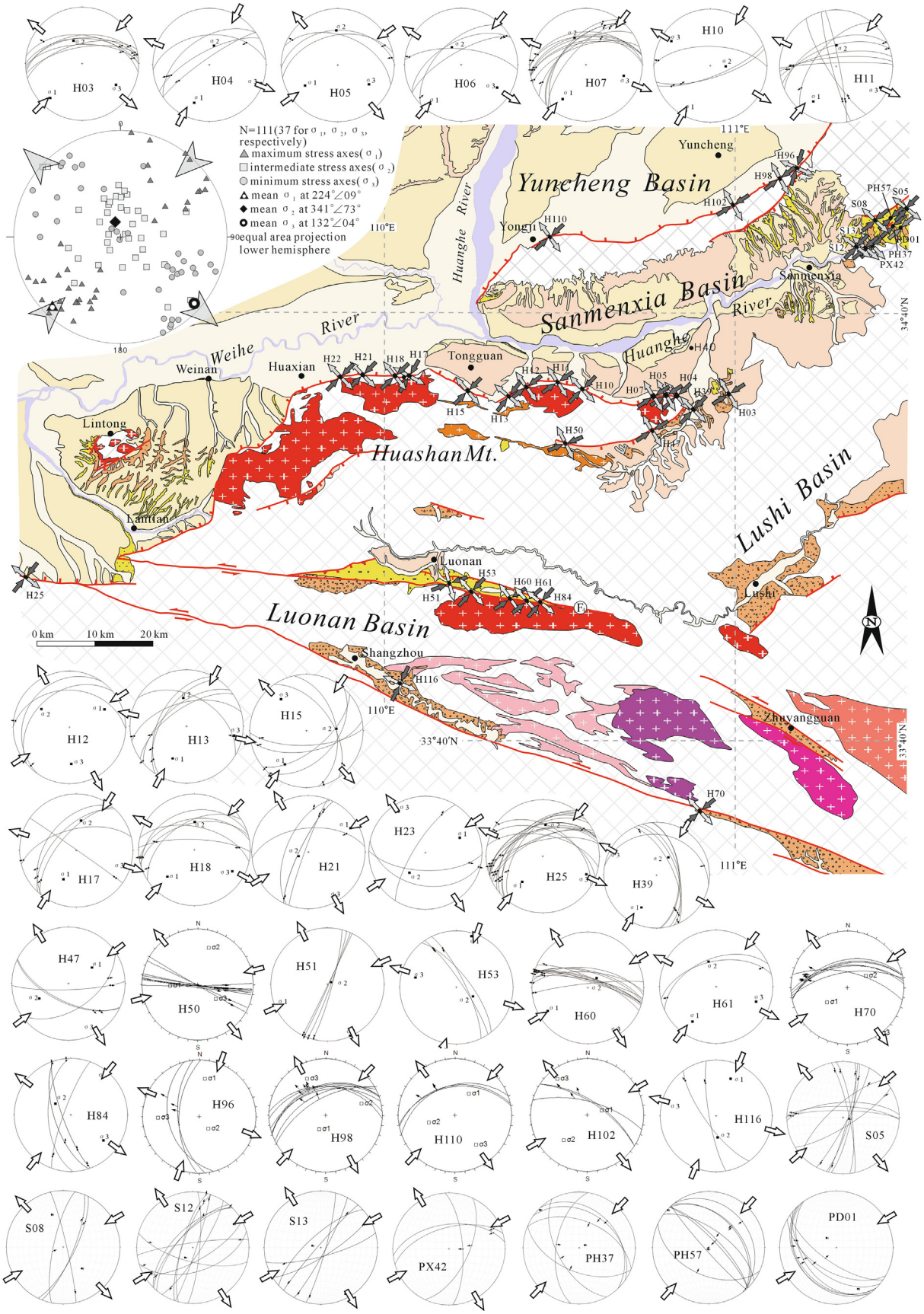


**Fig. 10.** The Late Miocene-Early Pleistocene transtensional stress regime (NW-SE extension and NE-SW compression) in the north margin of the Eastern Qinling Mountains, as shown by Lower-hemisphere, equal-angle (Wulff) stereographic plots of fault slip vectors. The opposing gray arrows present the minimum principal stress ($\sigma_3$) direction. Same legends as Fig. 2. The stereograms are also calculated as showed in Fig. 8.

**Table 3**
Slip vectors on fault planes measured in the north periphery of the Eastern Qinling Mountains and their NE-SW extensional stress field.

| Site | Longitude (E) | Latitude (N) | Stratigraphy-lithology | Vector number | $\sigma_1$ (az°/pl°) | $\sigma_2$ (az°/pl°) | $\sigma_3$ (az°/pl°) |
|---|---|---|---|---|---|---|---|
| H03 | 110°58′08″ | 34°29′30″ | gneiss fault facet | 7 | 223/18 | 340/54 | 122/30 |
| H04 | 110°48′43″ | 34°29′17″ | gneiss fault facet | 4 | 202/28 | 014/61 | 110/03 |
| H05 | 110°47′17″ | 34°29′08″ | gneiss fault facet | 3 | 238/32 | 358/38 | 122/35 |
| H06 | 110°45′52″ | 34°29′06″ | granite fault facet | 4 | 219/13 | 332/61 | 123/25 |
| H07 | 110°45′22″ | 34°28′47″ | granite fault facet | 12 | 214/27 | 337/47 | 106/31 |
| H10 | 110°33′23″ | 34°29′55″ | granite fault facet | 3 | 209/10 | 093/68 | 302/20 |
| H11 | 110°29′09″ | 34°30′39″ | marble fault facet | 9 | 213/27 | 001/59 | 116/14 |
| H12 | 110°24′10″ | 34°29′50″ | granite fault facet | 3 | 063/30 | 303/40 | 177/35 |
| H13 | 110°21′33″ | 34°28′43″ | gneiss fault facet | 6 | 203/38 | 354/48 | 101/15 |
| H15 | 110°14′11″ | 34°2907″ | gneiss fault facet | 6 | 213/30 | 086/46 | 321/29 |
| H17 | 110°03′25″ | 34°31′10″ | gneiss fault facet | 5 | 204/44 | 009/46 | 107/07 |
| H18 | 110°01′56″ | 34°31′02″ | gneiss fault facet | 6 | 225/32 | 001/49 | 120/23 |
| H21 | 109°56′25″ | 34°30′56″ | gneiss fault facet | 5 | 060/15 | 247/75 | 151/02 |
| H23 | 109°52′41″ | 34°31′06″ | gneiss fault facet | 3 | 067/34 | 218/53 | 327/14 |
| H25 | 109°00′41″ | 34°01′14″ | gneiss fault facet | 16 | 219/42 | 005/43 | 113/17 |
| H39 | 110°51′50″ | 34°27′07″ | $Q_2$conglomerate | 6 | 205/33 | 034/57 | 298/04 |
| H47 | 110°45′28″ | 34°25′00″ | gneiss fault facet | 4 | 056/48 | 243/42 | 150/03 |
| H50 | 110°30′57″ | 34°22′14″ | granite fault facet | 8 | 263/43 | 122/38 | 018/20 |
| H51 | 110°11′46″ | 34°02′41″ | N conglomerate | 4 | 246/06 | 060/84 | 156/01 |
| H53 | 110°14′32″ | 34°02′26″ | E conglomerate | 3 | 017/06 | 119/63 | 284/27 |
| H60 | 110°23′37″ | 34°00′17″ | granite fault facet | 12 | 240/18 | 043/71 | 148/05 |
| H61 | 110°26′03″ | 34°00′00″ | granite fault facet | 2 | 214/26 | 343/52 | 111/25 |
| H70 | 110°53′58″ | 33°31′11″ | Econglomerate | 7 | 238/41 | 052/58 | 145/03 |
| H84 | 109°59′53″ | 34°03′52″ | E sandstone | 6 | 038/01 | 306/63 | 128/27 |
| H96 | 111°09′36″ | 35°00′41″ | gneiss fault facet | 3 | 006/20 | 144/63 | 270/16 |
| H98 | 111°06′15″ | 34°59′19″ | gneiss fault facet | 8 | 211/60 | 069/23 | 332/15 |
| H102 | 110°57′09″ | 34°54′49″ | gneiss fault facet | 3 | 065/61 | 225/27 | 320/08 |
| H110 | 110°27′28″ | 34°50′41″ | gneiss fault facet | 3 | 028/40 | 258/37 | 144/27 |
| H116 | 110°04′30″ | 33°47′10″ | $K_2$ sandstone | 2 | 21/29 | 176/58 | 285/11 |
| S05 | 111°28′54″ | 34°55′17″ | $N_1$ sandstone | 11 | 231/06 | 101/81 | 322/07 |
| S08 | 111°06′09″ | 34°55′46″ | $N_1$ conglomerate | 4 | 242/11 | 139/49 | 341/39 |
| S12 | 111°21′55″ | 34°49′55″ | $E_3$ sandstone | 12 | 060/17 | 219/72 | 328/06 |
| S13 | 111°20′30″ | 34°50′08″ | $N_2$ sandstone | 6 | 061/10 | 283/77 | 152/08 |
| PX42 | 111°20′43″ | 34°50′38″ | $E_{2-3}$ conglomerate | 4 | 223/02 | 132/07 | 326/83 |
| PH37 | 111°31′11″ | 34°56′07″ | $E_3$-$N_1$ mudstone | 6 | 224/09 | 314/03 | 063/81 |
| PH57 | 111°31′04″ | 34°54′01″ | $E_3$-$N_1$ mudstone | 8 | 042/03 | 312/01 | 195/87 |
| PD01 | 111°26′39″ | 34°52′09″ | $E_{2-3}$ mudstone | 7 | 056/03 | 146/13 | 313/77 |

$\sigma_1$, $\sigma_2$, $\sigma_3$ correspond to maximum, intermediate, and minimum compressive stress, respectively; az°-azimuth, pl°-plunge, $R=(\sigma_2-\sigma_3/\sigma_1-\sigma_3)$; $K_2$-Upper Cretaceous, E-Paleocene, $E_{2-3}$-Eocene-Oligocene, $E_3$-$N_1$-Oligocene-Miocene, N-Neocene, $N_1$-Miocene, $N_2$-Pliocene, $Q_2$-Middle Pleistocene.

wall composed of Late Pleistocene loess in part, and marked by fault facets. A set of striations on the fault facet indicates the NNW-SSE extension (Fig. 5A). A fault cuts the Eocene medium- to thin-bedding mudstone and Late Pleistocene loess with the OSL age of 36.3 ka at Loc. S14 near the Yellow River (the location in Fig. 8), where one generation of striations delimit ~N–S extension, as calculated from fault slip vectors (Fig. 5B). At Loc. PX12 to the east of the Sanmenxia dam (location shown in Fig. 11), A fault zone with the width of the 100 cm was exposed the Eocene massive silty mudstone, and overlain by the Late Pleistocene loess (Fig. 5C). There are two sets of striations on the fault plane, including normal dip-slip activity and oblique slip striations, indicating early NW-SE extensional and nearly S-N extension, respectively (Fig. 5C). At Loc. P20 east of the Sanmenxia Basin, a group of syn-sedimentary normal faults with a trend/dip of 355°∠49° cut the Late Pleistocene gravel and sand deposits, suggesting a NE-SW extensional activity in the Late Pleistocene, as delimited by the fault kinematics (Fig. 5D). To the south of the Sanmenxia dam (Loc. S15; location shown in Fig. 12), the Middle-Late Miocene medium- to thin-bedding sandstones were cut by a series of normal faults with the striking of NE direction. The fault kinematics analysis indicates a NW-SE extensional activity prior to the Holocene, coupled with deposits of Holocene sandy clay overlying the fault (Fig. 5E). Locally a syn-sedimentary normal fault also developed in the medium- to thick-bedding sandstones of the Middle-Late Miocene with a trend/dip of 133°∠34°, generally indicating NW-SE extensional deformation in the Middle-Late Miocene (Fig. 5F). At the Loc. S07, the northeast of the basin, a normal fault grew in the Oligocene thick-bedding red mudstone and pebbly sandstone, with the offset of ~60 cm. The fault slip vector analysis shows a NW-SE extensional deformation prior to the Late Pleistocene, together with the deposits of Late Pleistocene covering the fault (Fig. 5G). At piedmont of Zhongtiao Mt. the east of the basin (Loc. S09), the Eocene thin-bedding mudstones are marked by strongly folding, Here the folding analysis largely indicates that an early NW-SE and NE-SW shortening deformations occurred in or posterior the Eocene (Fig. 5H), denoting the Sanmenxia Basin has undergone two-phase shortening deformations in the Cenozoic.

Thus, our structural analysis outlines at least four alternating episodes of shortening and extensional deformation in the Sanmenxia Basin, the NW-SE extension, NW-SE shortening, NE-SW shortening, NE-SW extension, and NNW-SSE extension, orderly.

### 3.3. The south margin of Yuncheng Basin

The Zhongtiaoshan Piedmont Fault ($F_3$) bounds the southern Yuncheng Basin, and has well-exposed fault facets (Fig. 6A). At the Loc. H93 along the Zhongtiaoshan Piedmont Fault, the boundary fault is featured by Neoproterozoic granite in the footwall and Late Pleistocene loess in the hanging wall, showing an NW-SE extensional deformation, as indicated by its dip-slip fault vectors, probably representing early activity. Here the normal faulting in the Late Pleistocene loess of hanging wall coincides with NE-SW extension in or posterior to Late Pleistocene, as deduced from fault kinematic analysis (Fig. 6B). The Late Miocene-Pliocene red clay was deposited along the east segment of the Zhongtiaoshan Piedmont Fault (Wang et al., 2002), where a set of normal faults was exposed at Loc. H92. The fault kinematic analysis, together with an examination of the crosscutting relationships of the

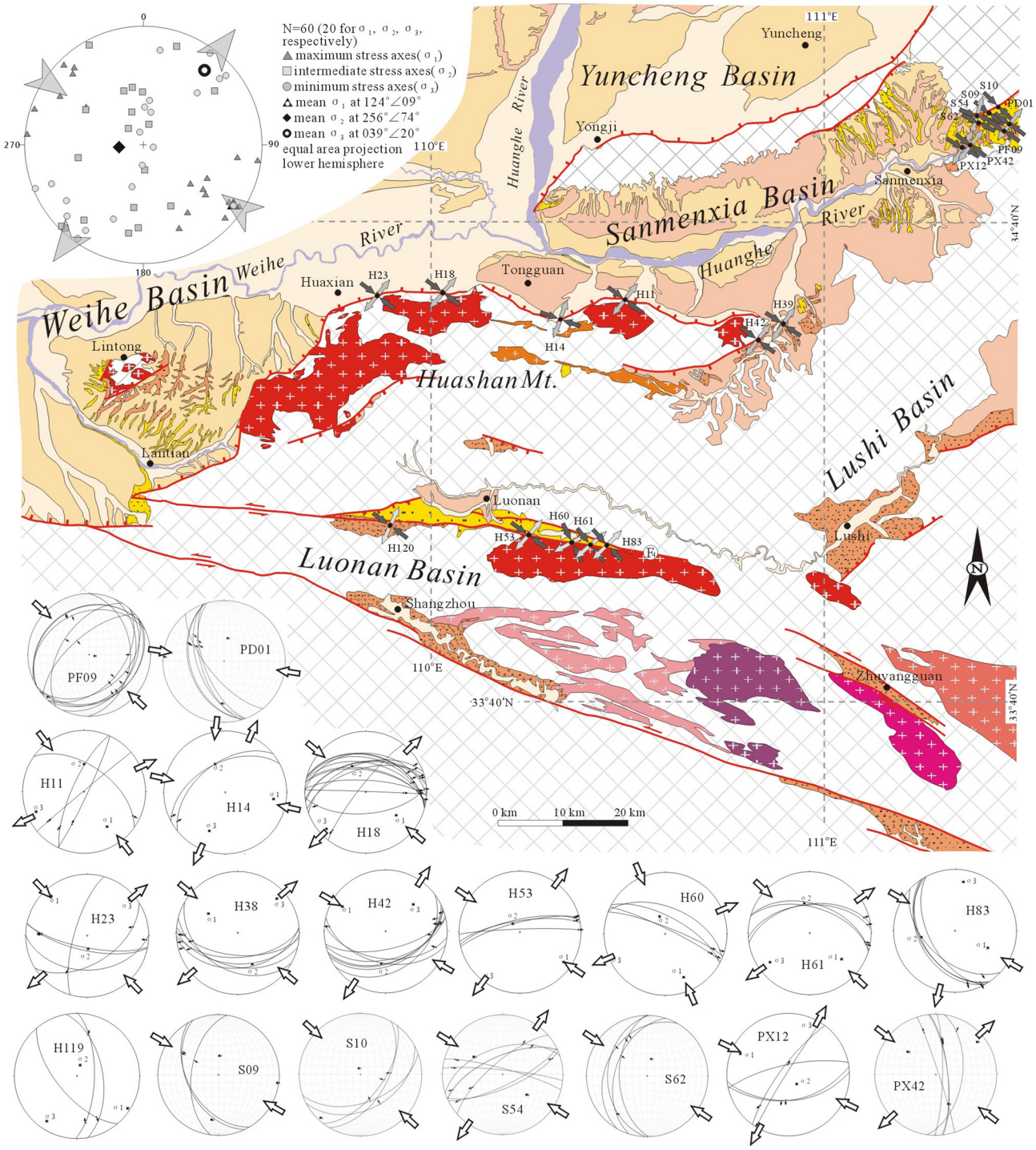


**Fig. 11.** The Late Miocene transtensional stress field (NW-SE compression and NE-SW extension) in the north periphery of the Eastern Qinling Mountains, inferred from fault-slip vectors. Same legends as Fig. 2. The stereograms are also calculated as showed in Fig. 8.

faults, indicates dip-slip and subsequent oblique-slip activity, related to early NW–SE extension and later ~N-S extension, respectively (Fig. 6C; Shi et al., 2015b). At H97 near the Zhongtiaoshan Piedmont Fault (the location in Fig. 8), a cluster of high-angle normal faults cut Late Pleistocene loess and gravel-bearing sandy clay, which is linked with Late Pleistocene or later NNW-SSE extension according to fault kinematics analysis (Fig. 6D), denoting that this period of extension occurred in the Late Pleistocene or later.

The above deformation analysis of the boundary faults along the southern margin of the Yuncheng Basin, combined with the previous structural investigation in the Shanxi Basin (Shi et al., 2015b), delimits that three stages of extensional deformation successively occurred in the Yuncheng Basin since the Cenozoic, i.e., the NW-SE, NE-SW, and NNW-SSE extensions.

### 3.4. Luonan and Lushi Basins

The Luonan Basin developed on the northern margin of the East Qinling Mts., and is controlled by the N-W Luonan-Luanchuan ($F_4$) and the Shang-Dan faults ($F_5$) to the south (Fig. 2). At Loc. H51 (the location shown in Fig. 8) in the interior of the Luonan Basin, a suite of normal faults grew in the Neogene red medium- to thin-bedding mudstone in

**Table 4**
A NW-SE contractional stress field calculated from fault slip vector measured in the north periphery of the Eastern Qinling Mountains.

| Site | Longitude (E) | Latitude (N) | Stratigraphy-lithology | Vector number | $\sigma_1$ (az°/pl°) | $\sigma_2$ (az°/pl°) | $\sigma_3$ (az°/pl°) |
|---|---|---|---|---|---|---|---|
| H11 | 110°29′09″ | 34°30′39″ | marble fault facet | 4 | 147/32 | 000/53 | 247/17 |
| H14 | 110°19′17″ | 34°27′49″ | gneiss fault facet | 2 | 098/21 | 341/50 | 202/33 |
| H18 | 110°01′56″ | 34°31′02″ | gneiss fault facet | 15 | 127/37 | 332/50 | 227/13 |
| H23 | 109°52′41″ | 34°31′06″ | gneiss fault facet | 5 | 318/14 | 175/73 | 050/10 |
| H38 | 110°51′00″ | 34°27′33″ | gneiss fault facet | 6 | 303/42 | 155/43 | 49/16 |
| H42 | 110°49′13″ | 34°26′03″ | gneiss fault facet | 8 | 300/20 | 188/46 | 046/37 |
| H53 | 110°14′32″ | 34°02′25″ | N conglomerate | 4 | 124/14 | 320/75 | 215/04 |
| H60 | 110°23′37″ | 34°00′37″ | granite fault facet | 4 | 157/24 | 342/66 | 248/02 |
| H61 | 110°26′03″ | 33°59′59″ | granite fault facet | 4 | 129/33 | 350/49 | 234/21 |
| H83 | 109°59′50″ | 34°03′31″ | E conglomerate | 5 | 118/39 | 259/44 | 010/20 |
| H119 | 109°53′29″ | 34°03′12″ | $N_1$ conglomerate | 3 | 123/04 | 17/75 | 214/14 |
| S09 | 111°22′25″ | 34°52′12″ | $E_{2-3}$ mudstone | 3 | 98/03 | 189/26 | 002/64 |
| S10 | 111°26′10″ | 34°53′10″ | $E_{2-3}$ mudstone | 4 | 132/08 | 223/05 | 344/81 |
| S54 | 111°08′10″ | 34°56′40″ | $E_{2-3}$ sandstone | 7 | 130/47 | 302/43 | 036/05 |
| S62 | 111°06′15″ | 34°53′20″ | $E_2$ conglomerate | 4 | 125/09 | 218/21 | 013/67 |
| PX12 | 111°20′30″ | 34°50′05″ | $E_2$ conglomerate | 5 | 288/04 | 019/13 | 183/76 |
| PX42 | 111°20′43″ | 34°50′38″ | $E_{2-3}$ conglomerate | 5 | 315/17 | 053/25 | 195/60 |
| PF09 | 111°20′12″ | 34°46′10″ | $E_{2-3}$ mudstone | 12 | 315/06 | 225/04 | 103/83 |
| PD01 | 111°26′39″ | 34°52′09″ | $E_{2-3}$ mudstone | 6 | 275/02 | 183/31 | 008/59 |

$\sigma_1$, $\sigma_2$, $\sigma_3$ correspond to maximum, intermediate, and minimum compressive stress, respectively; az°-azimuth, pl°-plunge, R = ($\sigma_2$-$\sigma_3$/$\sigma_1$-$\sigma_3$); E-Paleocene, $E_{2-3}$-Eocene-Oligocene, $E_3$-$N_1$-Oligocene-Miocene, N-Neocene, $N_1$-Miocene.

the interval of white thick-bedding conglomerate with a normal offset of ~30 cm (Fig. 7A). The kinematic analysis shows a ~N-S extension deformation in this area. To the south of the Luonan Basin (Loc. H74), a group of normal faults cut the Paleogene thick-bedding red sandstone sandwiched with a thin-bedding red conglomerate with the horizontal bedding (S0: 98°∠06°), where fault striations indicate a NE-SW extensional deformation (Fig. 7B). At Loc. H82 northwest of the Luonan Basin, a series of normal faults can be observed in the Neogene medium- to thin-bedding red mudstones (Fig. 7C), documenting early NE-SW extension and later ~N-S extension in the Neogene or later, as revealed by the fault slip vectors, and coupled with the crosscutting relationships of the two groups of the striations (Fig. 7D). At the middle segment of the Shang-Dan fault (Loc. H73), a set of normal faults cut the Paleogene red medium- to thin-bedding pebble-bearing sandstone with a bedding ($S_0$) orientation of 47°∠33° (Fig. 7E). Here the faulting is as well represented as early NE-SW and later N-S extensional activity, as indicated by fault normal dip-slip and oblique-slip vectors, and together with the crosscutting superposed relationships of the striations (Fig. 7F). At Loc. H68, east segment of the Shang-Dan fault, a fault in the Paleogene gray-white thick-bedding conglomerates is featured by old normal dip-slip striations and right-lateral strike-slip striations, indicating early NE-SW extension and later NNW-SSE extension (Fig. 7G). A large fault was exposed in the east of Lushi County (Loc. H67), with the footwall of the Paleogene gray mudstone, and the hanging wall of the Late Pleistocene loess (Fig. 7H), where normal dip-slip motion of the fault coincides with NNW-SSE extension, as deduced by fault vector analysis.

The above-mentioned analysis of some out-crops examples shows that the NW-SE, NE-SW, and ~N-S extensional deformations have orderly dominated this area since the late Cenozoic.

## 4. Cenozoic paleostress sequences

A stress field is customarily stabilized in a given region in a certain period, in favor of establishing stress field sequences on the basis on fault kinematic analysis, further to define the tectonic evolution history of a region (e.g. Mercier et al., 1991; Zhang et al., 2003; Shi et al., 2012). To understand the Cenozoic tectonic stress regimes in the northern margin of the East Qinling Mts., our structural investigation was conducted on the Cenozoic basins in the region as analyzed above, and coeval with geochronological results, we orderly reconstruct five-stage tectonic stress field in the basins, marked by the episodic changes of principal stress directions as follows: (1) ~N-S extension since the end of the Late Pleistocene (Fig. 8; Table 1), (2) the Late Pleistocene NE-SW extension (Fig. 9; Table 2), (3) the Late Miocene–Early Pleistocene NE-SW compression (Fig. 10; Table 3), (4) the Late Miocene NW-SE compression (Fig. 11; Table 4), and (5) the Oligocene–Middle Miocene NW-SE extension (Fig. 12; Table 5).

### 4.1. The ~N-S extension since the end of the Late Pleistocene

The fault kinematic analysis on the basin boundary fault described above, coupled with our previous studies on the Shanxi rift basins (Shi et al., 2015a), and the recent structural investigation (Rao et al., 2014), reveals a NNW-SSE extension event in the north of East Qinling Mt. since the end of the Late Pleistocene, featured by the mean stress orientations of 117°/79° for $\sigma_1$, 263°/08° for $\sigma_2$, 354°/07° for $\sigma_3$, as calculated from the structural data at numerous individual sites (Fig. 8; Table 1). Our structural analysis exhibits Holocene sandy clay is the youngest strata involved in this extensional stage, representing the youngest deformation in this region. The focal mechanisms of earthquakes (IG and SBNHAP, 1990; Guo et al., 2017), together with GPS (Wang et al., 2001; Gao et al., 2017), reveals sub-horizontal NNW–SSE extensional activity in this region, denoting that this extensional event has probably lasted to the present day.

### 4.2. The Late Pleistocene NE–SW extension

Our structural analysis shows that the subsequent paleostress is characteristic of a weaker NE–SW extension, with a regional $\sigma_1$ at 320°/80°, $\sigma_2$ at 115°/08°, $\sigma_3$ at 231°/04° (Fig. 9; Table 2). This extension coincides with the Late Pleistocene deposit process, as confirmed above (Fig. 5D; Shi et al., 2015a), suggesting that the extension event occurred in the Late Pleistocene.

### 4.3. The late Miocene–Early Pleistocene NE-SW compression

The paleostress inversion analyses are performed at 35 sites, determining a regional compressive stress regime with the mean principal stress direction characteristic of 224°/09°, 341°/73, 132°/04° (Fig. 10, Table 3). The studies on the late Cenozoic tectonic stress regime in the Shanxi Rift show the compression controlled the Late Miocene–Early Pleistocene structures, in accordance with that of the west margin of the Ordos Block (Xie et al., 2000; Shi et al., 2015b).

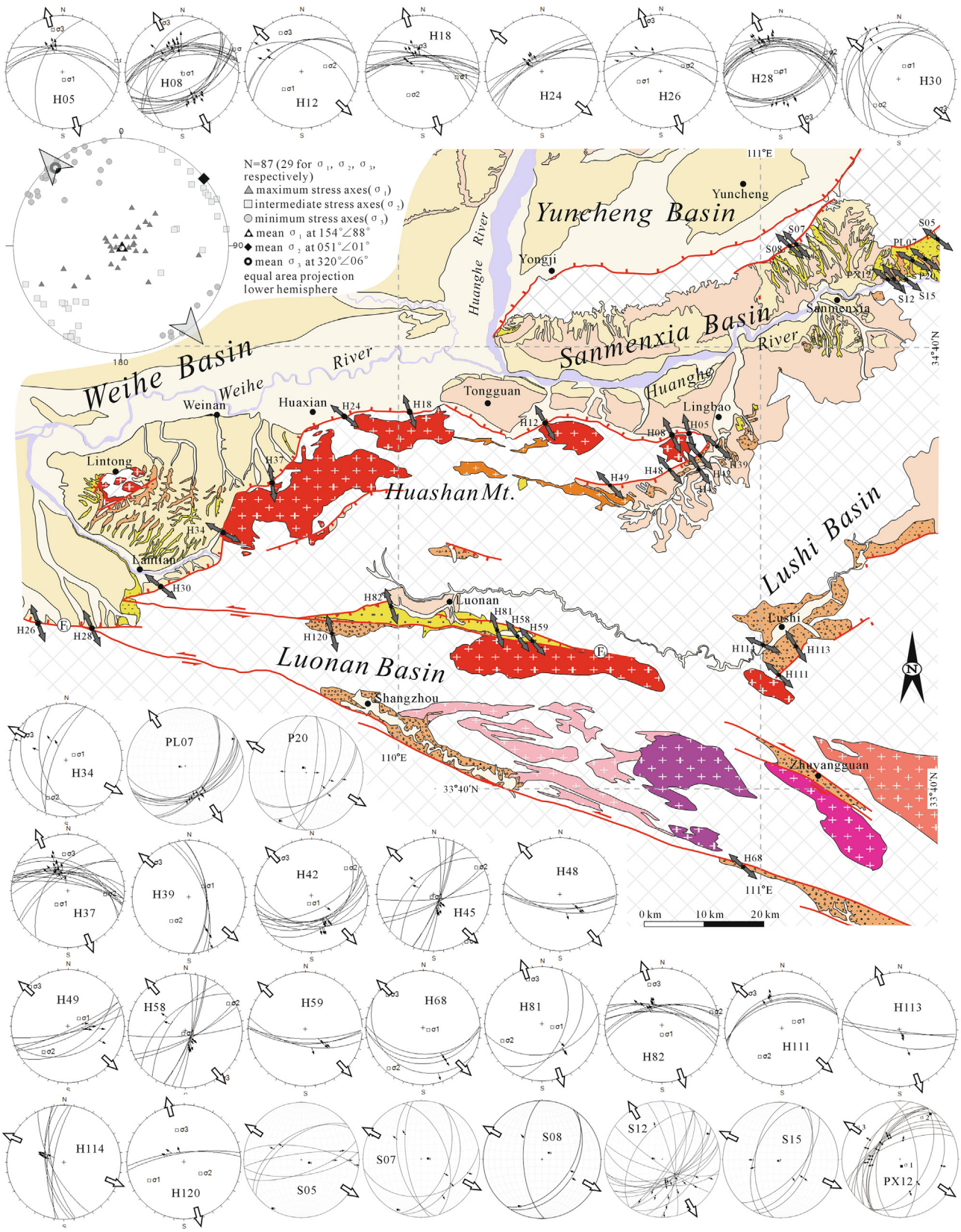


**Fig. 12.** The Oligocene-Middle Miocene NW-SE extension in the north periphery of the Eastern Qinling Mountains, resulted from the analysis of fault-slip vectors. Same legends as Fig. 2. The stereograms are also calculated as showed in Fig. 8.

**Table 5**
Results of fault-slip analysis and stress orientations in the north periphery of the Eastern Qinling Mountains, revealing a NW-SE extensional stress regime.

| Site | Longitude (E) | Latitude (N) | Stratigraphy-lithology | Vector number | $\sigma_1$ (az°/pl°) | $\sigma_2$ (az°/pl°) | $\sigma_3$ (az°/pl°) |
|---|---|---|---|---|---|---|---|
| H05 | 110°47′17″ | 34°29′08″ | gneiss fault facet | 13 | 080/80 | 238/09 | 329/03 |
| H08 | 110°44′49″ | 34°28′37″ | granite fault facet | 21 | 188/89 | 064/01 | 334/01 |
| H10 | 110°33′23″ | 34°29′55″ | granite fault facet | 3 | 189/89 | 081/01 | 351/01 |
| H12 | 110°24′10″ | 34°29′50″ | granite fault facet | 4 | 229/42 | 073/45 | 331/12 |
| H18 | 110°01′56″ | 34°31′02″ | gneiss fault facet | 8 | 097/28 | 212/38 | 341/38 |
| H24 | 109°51′18″ | 34°30′25″ | gneiss fault facet | 7 | 143/55 | 043/06 | 309/33 |
| H26 | 109°02′76″ | 34°00′59″ | gneiss fault facet | 4 | 248/42 | 073/47 | 340/02 |
| H28 | 109°01′24″ | 34°00′08″ | gneiss fault facet | 18 | 295/77 | 064/07 | 155/09 |
| H30 | 109°22′36″ | 34°06′25″ | gneiss fault facet | 6 | 016/60 | 224/26 | 128/11 |
| H34 | 109°32′01″ | 34°14′21″ | granite fault facet | 6 | 044/71 | 208/17 | 299/04 |
| H37 | 109°39′47″ | 34°20′25″ | gneiss fault facet | 14 | 226/55 | 093/25 | 352/22 |
| H39 | 110°51′50″ | 34°27′07″ | E conglomerate | 4 | 047/54 | 219/34 | 311/04 |
| H42 | 110°50′23″ | 34°25′29″ | gneiss fault facet | 9 | 208/74 | 049/14 | 318/05 |
| H45 | 110°49′34″ | 34°24′21″ | E conglomerate | 10 | 240/82 | 055/07 | 145/01 |
| H48 | 110°44′19″ | 34°24′20″ | gneiss fault facet | 4 | 024/54 | 171/30 | NW-SE |
| H49 | 110°34′35″ | 34°22′23″ | gneiss fault facet | 6 | 046/64 | 226/25 | 316/01 |
| H58 | 110°20′00″ | 34°01′21″ | N conglomerate | 9 | 057/78 | 233/11 | 323/01 |
| H59 | 110°22′40″ | 34°00′41″ | E conglomerate | 4 | | | NW-SE |
| H68 | 110°57′09″ | 33°30′50″ | E conglomerate | 4 | 104/84 | 222/04 | 312/07 |
| H81 | 110°17′34″ | 34°01′42″ | N conglomerate | 3 | 103/71 | 248/05 | 341/09 |
| H82 | 109°59′32″ | 34°04′57″ | N conglomerate | 8 | 188/73 | 073/07 | 314/14 |
| H111 | 111°02′30″ | 33°56′44″ | E conglomerate | 4 | 054/63 | 220/25 | 313/05 |
| H113 | 110°05′10″ | 34°00′32″ | E conglomerate | 3 | | | NW-SE |
| H114 | 110°59′47″ | 34°00′41″ | E conglomerate | 6 | | | NW-SE |
| H120 | 109°50′04″ | 34°00′57″ | E conglomerate | 3 | 244/19 | 124/53 | 345/28 |
| S05 | 111°28′54″ | 34°55′17″ | $N_1$ sandstone | 6 | 110/78 | 211/02 | 301/11 |
| S07 | 111°06′14″ | 34°55′58″ | $N_1$ mudstone | 6 | 087/81 | 205/04 | 296/08 |
| S08 | 111°06′09″ | 34°55′46″ | $N_1$ conglomerate | 3 | 036/82 | 209/08 | 299/01 |
| S12 | 111°21′55″ | 34°49′55″ | $E_3$ sandstone | 21 | 286/79 | 058/08 | 150/08 |
| S15 | 111°18′48″ | 34°49′25″ | $N_2$ sandstone | 5 | 251/86 | 023/03 | 113/03 |
| PX12 | 111°20′30″ | 34°50′05″ | Fault | 15 | 167/80 | 034/07 | 303/08 |
| PL07 | 111°25′29″ | 34°53′30″ | $E_{2-3}$ mudstone | 10 | 266/82 | 060/07 | 151/04 |
| P20 | 111°23′35″ | 34°53′05″ | $E_{2-3}$ mudstone | 6 | 329/82 | 209/04 | 118/07 |

$\sigma_1$, $\sigma_2$,$\sigma_3$ correspond to maximum, intermediate, and minimum compressive stress, respectively; az°-azimuth, pl°-plunge, $R=(\sigma_2-\sigma_3/\sigma_1-\sigma_3)$; E-Paleocene, $E_{2-3}$-Eocene-Oligocene, $E_3$-$N_1$-Oligocene-Miocene, N-Neocene, $N_1$-Miocene, $N_2$-Pliocene.

### 4.4. The Middle-Late Miocene NW-SE compression

The structural investigation shows that the NW-SE compressive structures develop in the basins along the east Qinling except for the Yuncheng Basin. The stress field inversion from the fault data reveals a compressive stress regime, marked by the directions of three principle stress axis (124°/09° for $\sigma_1$, 256°/74° for $\sigma_2$, 039°/20° for $\sigma_3$) (Fig. 10, Table4). The compression led to the folding of the Eocene-Miocene clastic deposit as shown in the Sanmenxia Basin, and the sendimentary interval in the middle-upper Miocene strata (Chen et al., 2018), suggesting the compressive stress regime occurred in the Late Miocene, likely at ~10 Ma, as inferred from the Cenozoic paleostress analysis in the west margin of the Ordos Block (Shi et al., 2015b).

### 4.5. The oligocene–middle miocene NW-SE extension

The fault kinematic studies conclude a followed extensional stress regime, marked by the mean principal stress directions of 154°/88° for $\sigma_1$, 051°/01° for $\sigma_2$, 320°/06° for $\sigma_3$, as calculated from the structural data at numerous individual sites from the Weihe, Sanmenxia, Luonan basins (Fig. 12, Table5), indicating NW-SE extension. The development of syn-sedimentary structures in the Middle-Late Miocene rocks from the Sanmenxia Basin limits the extension occurred in the Middle-Late Miocene as described above; and the analysis of Cenozoic deformation in the Weihe Basin shows the NW-SE extension dominated the sedimentation of the Middle-Late Miocene Bahe Fm. (Bellier et al., 1988). Together with the previous Cenozoic paleostress inversions around the Ordos Block (Zhang et al., 2006; Huang et al., 2013; Shi et al., 2015b), we deduce the extensional regime is the oldest stress field which affected this region, from the Eocene to Late Miocene.

## 5. Discussion: Cenozoic tectonic process

The Cenozoic faulted basins on the north margin of the Eastern Qinling, situated at the intersection area of the Taihangshan tectonic belt and the Qinling orogenic belt (Li et al., 2015), which is likely affected by the eastward expansion of the Tibetan Plateau and the westward subduction of the Pacific Plate (Zhang et al., 2006), leading to the complex tectonic evolution process of the basin system in the Cenozoic. Here comparison of the Cenozoic sediment sequences of the basins shows the Paleocene sandstone and conglomerate is the oldest deposits filled in the Sanmenxia, Luonan and Lushi Basins (BGMSNX, 1989; BGMHN, 1989), and the Eocene sandstone and conglomerate in the Weihe Basin named as the Honghe Formation (Li et al., 2016); the oldest strata deposit in the Yuncheng Basin is the Middle-Late Miocene-Pliocene red clay named as the Jingle Formation (Wang et al., 2002), which largely suggest a two-stage tectono-sedimention process in the north periphery of eastern Qinling orogen, the formation of the Sanmenxia, Luonan, Lushi, and Weihe Basins in early stage, and the development of the Yuncheng Basin in the later stage.

Here the structural analyses on the Cenozoic basins delimits a five-phase Cenozoic deformation process mentioned above, coupled with the related tectonic stress fields inversed from fault kinematic analysis, suggest two stage of tectonic evolution in the north periphery of eastern Qinling orogen, comprising early pure-shear extension and faulted basin development in the Eocene-Middle Miocene and later dextral-shear deformation and formation of pull-apart basins during the Late Miocene-Holocene (Fig. 13).

**Stage I: Pure-shear extension and faulted basin development in the Paleocene-Middle Miocene**

The North China Plate, dominated by the NW-SE extensional stress field, was decomposed in the Paleocene-Middle Miocene, leading to

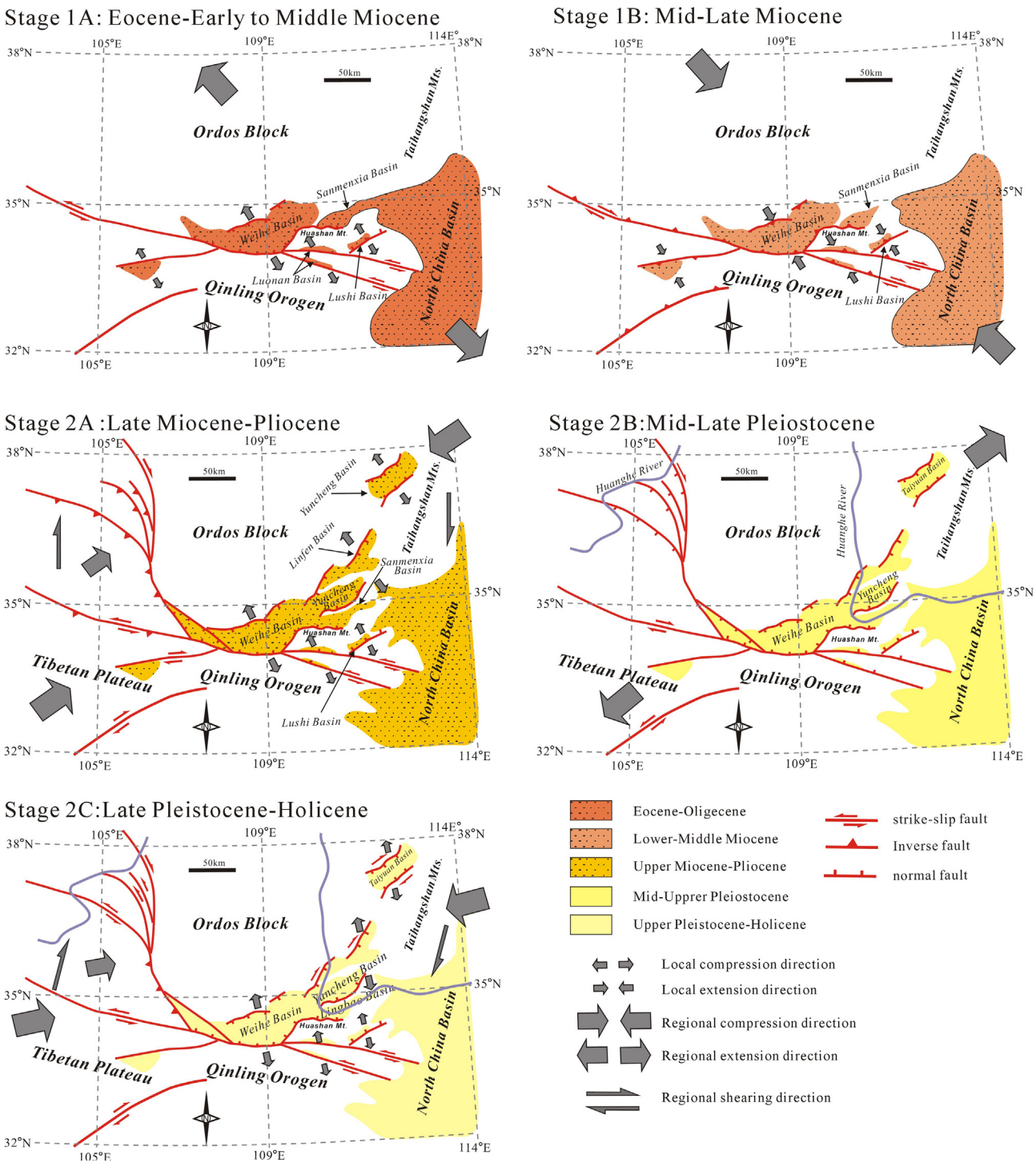


**Fig. 13.** Cenozoic tectonic evolution models in the north periphery of the Eastern Qinling Mountains. Stage 1A-The Eocene–Early-Middle Miocene faulted basin formation. Stage 1B-The Late Miocene faulted basin inversion. Stage 2A-The Late Miocene–Early Pleistocene strike-slip pull-part basin formation along the north periphery of Eastern Qinling Mountains. Stage 2B-The Late Pleistocene paleo-lake formation. Stage 2C-Strike-slip activity on the four major faults since the end of the Late Pleistocene. Stage B3-The Late Pleistocene-Holocene NNW-SSE extensional stress field in the north periphery of the Eastern Qinling Mountains.

widely the development of the Bohai Bay Basin (Hou et al., 2001). The extensional activity extended to the west, and effected on the interaction area of the Taihangshan structural belt and the East Qinling orogen, generating the Sanmenxia, Lushi, and Shangluo Basins in the interaction during the Paleocene-Middle Miocene (Zhang et al., 1978), sequentially the Weihe Basin along the Qinling Orogen in the Eocene-Middle Miocene (Fig. 13 Stage1A). The long-term extension was in accordance with the uplifting of the Qinling Mts. to the south of the basins, as revealed by the apatite fission-track studies (Wu et al., 2003; Hu et al., 2006; Liu et al., 2012; Chen et al., 2015), coinciding with the development of the Yinchuan Basin to the northwestern margin of the Ordos block (Huang et al., 2013). The dynamic origin is likely attributed to the northwestward subduction of the Pacific Plate (Isozaki et al., 2010). The Pacific slab was driven under the Taihang Mts., and the intersection of the Taihang Mts. and Qinling Mts. (Huang and Zhao, 2006), and was rolled back, causing the formation of the faulted basin

in the upper crust. Together with the regional stratigraphic sequence analysis, basin inversion occurred in the end of the Oligocene, likely 27–26.2 Ma, as limited by the Cenozoic sedimentary process (Chen et al., in review), which is probably related to the back-arc spreading from Pacific subduction (Otofuji et al., 1985). Then in the Early-Middle Miocene, the NW-SE extensional regime as well controlled the northern periphery of the Qinling Mts., the faulted basins are also featured by subsidence, and the expanding to the maximum extent. The following NW-SE compressive stress field has effect on the area during the Middle-Late Miocene, leading to basin inversion in the northern margin of the Qinling Mts. (Fig. 13 Stage1B), as indicated by an angular unconformity contact in the basin (Li et al., 2016; Chen et al., in review). This basin inversion is consistent with that on the west margin of the Ordos block (Chen et al., 2015; Shi et al., 2015b).

**Stage II: Dextral-shear deformation and formation of pull-apart basins during the Late Miocene-Holocene**

The previous structural investigation shows a NE-SW compressional stress dominated in this area in the Late Miocene to early Quaternary (~10–2.6 Ma) (Shi et al., 2015a), leading to a left-lateral strike-slip of the faults along the northern margin of the Qinling Mts., and a dextral strike-slip activities on the NE-striking faults in the Yuncheng region (Shi et al., 2015a). This regional strike-slip movement leads to the occurrence of Yuncheng Basin, as well to the lasting subsidence of the basins including the Weihe, Sanmenxia, Luonan, and Lushi Basins (Fig. 13 Stage 2A). The Qinling Mts. to the south margin of the basin strongly uplifted in this time, as well as the Luliang Mt. to the northern of the basin system, as reveled by fission track chronology (Wu et al., 2003; Chen et al., 2012; Liu et al., 2012). The recent tectono-sedimentation analysis shows that the northeastward growth of the Tibetan Plateau affected on the central part of the North China Plate in the Middle-Late Miocene (Zhang et al., 2006; Shi et al., 2006; Wang et al., 2011), and intensive crustal folding and shortening occurred in the western margin of the Ordos block at the end of the Pliocene (Shi et al., 2015b; Chen et al., 2015), denoting that the shear-extension in the northern margin of the Qinling Mts. was predominantly connected with India–Eurasia collision (Bao et al., 2013). However, it is also restricted by the Pacific Plate to the west (Park et al., 1998; Northrup et al., 1995), and probably attributed to a combinational effect of the Tibetan expanding to the west and Pacific retreating to the east (Li et al., 2010).

In the Middle-Late Pleistocene, the tectonic stress field was transformed into NE-SW extension (Shi et al., 2015a), which led to left-lateral striking slip on the basin boundary faults, sustained subsidence in the faulted basin, and the development of a large range of paleo-lakes within the basin (Fig. 13 Stage 2B). This west margin of the Ordos block also extensively developed NW-striking paleo-lakes at this stage under the extensional stress (Xu et al., 2013), characteristic of the phased uplift and expansion of the Tibetan Plateau.

Since the end of Late Pleistocene, a transtensional stress regime of NNW–SSE extension and WNW–ESE compression dominates on the northern margin of the Qinling Mountains (RGAFSO, 1988; Deng et al., 1999; Shi et al., 2015a, b), leading to the intensive left-lateral striking slip on the fault (Peltzer et al., 1985; Zhang et al., 1998). The Cenozoic basins are marked by extension and subsidence due to the intensive normal faulting on the basin boundary fault (Fig. 13 Stage 2C). This is consistent with the strong left-lateral striking-slip of NW-trending principal fault in the western margin of the Ordos block, which is predominantly linked with northeastward expansion of the Tibetan Plateau (Shi et al., 2015b); while the back-arc spreading of the Okinawa Trough (Park et al., 1998) also have an effect on this area.

## 6. Conclusions

(1) The fault kinematic analysis, together with the previous chronological data, delimits a two-phase Cenozoic tectonic process of the basins in the north of the East Qinling Mountains. The first stage is characteristic of a pure-shear extension and faulted basin development in the Paleocene-Middle Miocene, represented by the occurrence of the Sanmenxia, Lushi, Shangluo, and Weihe Basins along the East Qinling Mountains. The second stage is marked by dextral-shear deformation and formation of pull-apart basins (e.g. Yuncheng Basin) during the Late Miocene-Holocene.

(2) The faulted basins in the north of the East Qinling Mountains underwent the two phases of tectonic processes, likely in according with different dynamic backgrounds. The early basin development is attributed to the northwestward subduction of the Pacific Plate, and the late is originated from the far-field effect of outward growth of the Tibetan Plateau and subduction of the Pacific Plate.

## Declaration of interests

The authors declare that they have no known competing financial interests or personal relationships that could have appeared to influence the work reported in this paper

## Acknowledgments

This study was supported by research Grants from Chinese Geological Survey (CGS) (Nos. DD20160060, 1212011120100, 1212011220259) and National Natural Foundation of China(No. 41672203). We are very grateful to Editors Profs. Sanzhong Li, Gang Rao, Jianmin Hu, and anonymous reviewers for their critical, constructive comments to improve the manuscript.

## References

An, Z.S., Sun, D.H., Chen, M.Y., Sun, Y.B., Li, L., Chen, B.Q., 2000. Red clay sequences in Chinese loess Plateau and recorded paleoclimate events of the Late Tertiary. Quat. Sci. 20, 435–446.

Bao, H.Y., Guo, Z.F., Zhang, L.L., Huang, Y.P., 2013. Tectonic dynamics of eastern China since the formation of the Pacific plate. Adv. Earth Sci. 28, 337–346.

Bellier, O., Mercier, J.L., Vergely, P., Long, C.X., Ning, C.Z., 1988. Cenozoic sedimentary and tectonic evolution of the Weihegraben (Shaanxi Country, Northern China). Bull. Soc. Geol. Fr. 4, 979–994.

Bureau of Geology and Mineral Resources of Henan Province (BGMRHN), 1990. Regional Geology of Henan Province. Geological Publishing House, Beijing. pp. 1–722.

Bureau of Geology and Mineral Resources of Shaanxi Province (BGMRSNX), 1990. Regional Geology of Shaanxi Province. Geological Publishing House, Beijing. pp. 1–698.

Bureau of Geology and Mineral Resources of Shanxi Province (BGMSX), 1989. Regional Geology of Shanxi Province. Geological Publishing House, Beijing. pp. 1–698.

Chen, G., Ding, C., Xu, L.M., Zhang, H.R., Hu, Y.X., Yang, P., Li, N., Mao, X.N., 2012. Analysis on the thermal history and uplift process of Zijinshan intrusive complex in the eastern Ordos basin. Chinese J. Geophys. 55, 3731–3741.

Chen, H., Hu, J.M., Wu, G.L., Shi, W., Geng, Y.Y., Qu, H.J., 2015. Apatite fission-track thermochronological constraints on the pattern of late Mesozoic-Cenozoic uplift and exhumation of the Qinling Orogen, central China. J. Asian Earth Sci. 114, 649–673.

Cheng, Y.L., He, C.Q., Rao, G., Yan, B., Lin, A.M., Hu, J.M., Yu, Y.L., Yao, Q., 2018. Geomorphological and structural characterization of the southern Weihe Graben, central China: implications for fault segmentation. Tectonophysics 722, 11–24.

Deng, Q., Cheng, S., Min, W., Yang, G.Z., Ren, D.W., 1999. Discussion on Cenozoic tectonics and dynamics of Ordos block. J. Geomech. 5, 13–21.

Gao, L.X., Han, X.M., Dai, Y., Li, J., Yang, H.Y., 2017. Movement characteristics and present seimic behavior of the Ordos block. J. Geodesy Geodynam. 37, 349–354.

Geological Survey Bureau of Shanxi Province (GSBSX), 2007. Regional Geology of Houma (1:250000). Geological Publishing House, Beijing. pp. 1–465.

Guo, X.Y., Jiang, C.S., Wang, X.S., Tian, X., 2017. Characteristics of small to moderate focal mechanism solutions stress field of the circum-Ordos block. J. Geodesy Geodyn. 37, 675–685.

Han, J.M., Hus, J.J., Liu, T.S., Paepe, R., Vandenberghe, R.E., 1991. Magnetic properties of the Malan and Lishi Formations. Quatern. Sci. 11, 310–325.

Hou, G.T., Qian, X.L., Cai, D.S., 2001. The Tectonic Evolution of Bohai Basin in Mesozoic and Cenozoic Time. Acta Scientiarum Naturalium-Universitatis Pekinensis 37, 845–851.

Hou, J.J., Han, M.K., Zhang, B.Z., Chai, B.L., Han, H.Y., 1995. Geomorphic expressions of the activity along north Qinling Piedmont Fault zone in the Late Quaternary period. Acta Geographica Sinica 2, 138–146.

Hu, S.B., Raza, A., Min, K., Kohn, B.P., Reiners, P.W., Ketcham, R.A., Wang, J.Y., Gleadow, A., 2006. Late Mesozoic and Cenozoic thermotectonic evolution along a transect from the north China craton through the Qinling orogen into the Yangtze craton, central China. Tectonics 25, 1–15.

Huang, J., Zhao, D., 2006. High-resolution mantle tomography of China and surrounding regions. J. Geophys. Res. 111, 1–21.

Huang, X.F., Shi, W., Li, H.Q., Chen, L., Cen, M., 2013. Cenozoic tectonic evolution of the

Yinchuan Basin: constrains from the deformation of its boundary faults. Earth Sci. Front. 20, 199–210.
Kaakinen, A., Lunkka, J.P., 2003. Sedimentation of the Late Miocene Bahe Formation and its implications for stable environments adjacent to Qinling mountains in Shaanxi. China. J. Asian Earth Sci. 22, 67–78.
Institute of Geology, State Seismological Bureau (IG), Seismological Bureau of Ningxia Hui Autonomous Province (SBNHAP), 1990. Haiyuan Active Fault. Seismological Press, Beijing. pp. 1–286.
Isozaki, Y., Kazumasa, A., Nakama, T., Yanai, S., 2010. New insight into a subduction-related orogen: a reappraisal of the geotectonic framework and evolution of the Japanese Islands. Gondwana Res. 18, 82–105.
Jolivet, L., Davy, P., Cobbold, P., 1990. Right-lateral shear along the Northwest Pacific Margin and the India-Eurasia Collision. Tectonics 9, 1409–1419.
Liu, T.S., 1985. Loess and the Environment. China Ocean Press, Beijing, pp. 1–251.
Lu, Y.C., Prescott, J.R., Robertson, G.B., Hutton, J.T., et al., 1987. Thermo luminescence dating of the Malan loess at Zhaitang, China. Geology 15, 603–605.
Li, H., Yang, X., Friedrich, H., Li, H., 2008. High resolution magnetostratigraphy and deposition cycles in the Nihewan Basin (North China) and their significance for stone artifact dating. Quatern. Res. 69, 250–262.
Li, S.Z., Guo, L.L., Xu, L.Q., Somerville, I.D., Cao, X.Z., Yu, S., Wang, P.C., Suo, Y.H., Zhao, S.J., 2015. Coupling and transition of Meso-Cenozoic intracontinental deformation between the Taihang and Qinling Mountains. J. Asian Earth Sci. 114, 188–202.
Li, S.Z., Suo, Y.H., Dai, L.M., et al., 2010. Development of the Bohai Bay Basin and destruction of the North China Craton. Earth Sci. Front. 17, 064–089.
Li, S.Z., Suo, Y.H., Santosh, M., Dai, L.M., Liu, X., Yu, S., 2013. Mesozoic to Cenozoic intracontinental deformation and dynamics of the North China Craton. Geol. J. 48, 543–560.
Li, Y.L., Yang, J.C., Su, Z.Z., 1994. Neotectonic movement and palaeochannel evolution in Yuncheng Basin. Earthq. Res. Shanxi 1, 3–6.
Li, Z.C., Li, W.H., Li, Y.X., Li, Y.H., Han, W., 2016. Cenozoic stratigraphy and paleoenviroments in the Weihe area, Shaanxi Province. J. Stratigrap. 40, 168–179.
Liu, H.J., Xue, X.X., 2004. Discussion on the Cenozoic and its chronology in the Weihe River basin. J. Earth Sci. Environ. 26, 1–5.
Liu, J.H., Zhang, P.Z., Lease, R.O., Zheng, D.W., Wan, J.L., Wang, W.T., Zhang, H.P., 2012. Eocene onset and late Miocene acceleration of Cenozoic intra-continental extension in the North Qinling range–Weihe graben: insights from apatite fission track thermochronology. Tectonophysics 584, 281–296.
Mercier, J.L., Carey, E., Sebrier, M., Stein, S., 1991. Palaeostress determinations from fault kinematics: application to the Neotectonics of the Himalayas-Tibet and the Central Andes. Philos. Trans. Roy. Soc. Lond. 337, 41–52.
Min, L., Zhang, Z., Wang, X., Zheng, S., Zhu, G., 2006. The basal boundary of the Nihewan formation at the Taiergou section of Yangyuan, Hebei Province. J. Stratigr. 2, 103–108.
Molnar, P., Tapponnier, P., 1975. Cenozoic tectonics of Asia: effects of a continental collision. Science 189, 419–426.
Northrup, C.J., Royden, L.H., Burchfiel, B.C., 1995. Motion of the Pacific plate relative to Eurasia and its potential relation to Cenozoic extension along the eastern margin of Eurasia. Geology 23, 719–722.
Qi, Y., Xu, H.B., Zhang, J.X., Luo, J.H., 2011. Geochemistry, geochronology and geological significance of Gufengshan granodiorite in Linfen grabben basin. Geol. Rev. 57, 565–573.
Qiu, Z.X., 2000. Nihewan Fauna and Q/N boundary in China. Quatern. Sci. 2, 142–154.
Qiu, Z., Qiu, Z., 1995. Chronological sequence and subdivision of Chinese Neogene mammalian faunas. Palaeogeogr. Palaeoclimatol. Palaeoecol. 116, 41–70.
Otofuji, Y., Matsuda, T., Nohda, S., 1985. Opening mode of the Japan Sea inferred from the paleomagnetism of the Japan Arc. Nature 317, 603–604.
Park, J.O., Tokuyama, H., Shinohara, M., Suyehiro, K., Taira, A., 1998. Seismic record of tectonic evolution and backarc rifting in the Southern Ryukyu island arc system. Tectonophysics 294, 21–42.
Peltzer, G., Tapponnier, P., Zhang, Z., Xu, Z.Q., 1985. Neogene and Quaternary faulting in and along the Qinling Shan. Nature 317, 500–505.
Rao, G., Lin, A., Yan, B., Jia, D., Wu, X., 2014. Tectonic activity and structural features of intracontinental active normal faults in the Weihe Graben, central China. Tectonophysics 636, 270–285.
Ren, J.Y., Tamaki, K., Li, S.T., Zhang, J.X., 2002. Late Mesozoic and Cenozoic rifting and its dynamic setting in Eastern China and adjacent areas. Tectonophysics 344, 175–205.
Ren, J., Peng, J.B., Wang, F.Y., 2012. The research of deep structural features of Weihe basin and adjacent areas. Chinese J. Geophys. 55, 2939–2947.
Schellart, W.P., Lister, G.S., 2005. The role of the East Asian active margin in widespread extensional and strike-slip Deformation in East Asia. J. Geol. Soc. London 162, 959–972.
Shi, W., Cen, M., Chen, L., Wang, Y.C., Chen, X.Q., Li, J.Y., Chen, P., 2015a. Evolution of the late Cenozoic tectonic stress regime in the Shanxi Rift, central North China Craton inferred from new fault kinematic analysis. J. Asian Earth Sci. 114, 54–72.
Shi, W., Dong, S.W., Yuan, L., Hu, J.M., Chen, X.H., Chen, P., 2015b. Cenozoic tectonic evolution of the South Ningxia region, northeastern Tibetan Plateau inferred from new structural investigations and fault kinematic analyses. Tectonophysics 649, 139–164.
Shi, W., Zhang, Y.Q., Dong, S.W., Hu, J.M., Wiesinger, M., Ratschbacher, L., Jonckheere, R., Li, J.H., Tian, M., Chen, H., Wu, G.L., Qu, H.J., Ma, L.C., Li, H.L., 2012. Intracontinental Dabashan orocline, southwestern Qinling, Central China. J. Asian Earth Sci. 46, 20–38.
Shi, W., Zhang, Y.Q., Ma, Y.S., Liu, G., Wu, L., 2006. Formation and modification history of the Liupanshan basin on the southwestern margin of Ordos block and tectonic stress field evolution. Geol. China 33, 1066–1074.
Sun, J.M., Xu, L.L., 2007. River terraces in the Fen-Wei graben, central China, and the relation with the tectonic history of the India-Asia collision system during the quaternary. Quatern. Sci. 27, 20–26.
Tapponnier, P., Xu, Z.Q., Francoise, R., Meyerm, B., Nicolas, A., Gerard, W., Yang, J.S., 2001. Oblique stepwise rise and growth of the Tibetan Plateau. Science 294, 1671–1677.
The Research Group on Active Fault System around Ordos Massif, State Seismological Bureau (RGAFSO), 1988. Active Fault System around Ordos Massif. Seismological Press, Beijing. pp. 1–335.
Tong, Y.S., Li, X., Wang, Y.Q., 2005. A brief introduction to recent advance in the Paleogene studies. J. Stratigr. 29, 109–113.
Wang, W.T., Zhang, P.Z., Kirby, E., 2011. A revised chronology for Tertiary sedimentation in the Sikouzi basin: implications for the tectonic evolution of the northeastern corner of the Tibetan Plateau. Tectonophysics 505, 100–114.
Wang, B., Zheng, H.B., Wang, P., He, Z., 2013. The Cenozoic strata and depositional evolution of Weihe Basin: progresses and Problems. Adv. Earth Sci. 28, 1126–1135.
Wang, C.C., 1965. On the Weihe graben. Acta Geologica Sinica 2, 153–164.
Wang, N.L., Yang, J.C., Xia, Z.K., Mo, D.W., Li, Y.L., Pan, M., 1996. The Sediment in Cenozoic and Structural Landform in Shanxi Graben. Science Press, Beijing, pp. 1–409.
Wang, Q., Li, C.G., Tian, G.Q., Zhang, W.Z., Liu, C., Ning, L.Y., Cheng, Z.G., He, C.Y., Yue, J., 2002. Tremendous change of the earth surface system and tectonic setting of salt-lake formation in Yuncheng Basin since 7.1 Ma. Sci. China (Ser. D: Earth Sci.) 45, 111–122.
Wang, Q., Zhang, P.Z., Freymueller, J., Bilham, R., Larson, K.M., Lai, X.A., You, X.Z., Niu, Z.J., Wu, J.C., Li, Y.X., Liu, J.N., Yang, Z.Q., Chen, Q.Z., 2001. Present-day crustal deformation of China constrained by global positioning system measurements. Science 294, 574–577.
Wang, S.B., Jiang, F.C., Wu, X.H., Wang, S.M., Tian, G.Q., 2004. The connotation and significance of Sanmen formation. Quatern. Sci. 24, 116–123.
Wu, Z.H., Wan, J.L., Zhou, C.J., 2003. Cenozoic uplift and denudation history of Huashan Mountains: evidence from fission track thermo-chronology of Huashan granite. Geol. Sci. Technol. Inform. 22, 27–32.
Xie, F.R., Shu, S.B., Dou, S.Q., Zhang, S.M., 2000. Quaternary tectonic stress field in the region of Haiyuan-Liupanshan fault zone to Yinchuan fault-depression. Seismolog. Geol. 22, 139–146.
Xu, T., Yang, J.X., Liu, Y., Shi, W., Wei, W., 2013. The sedimentary characteristics in the Late Pleistocene in southern Ningxia and its tectonic significance. Earth Sci. Front. 20, 36–45.
Xu, X.W., Ma, X.Y., 1992. Geodynamics of the Shanxi Rift system, China. Tectonophysics 208, 325–340.
Xu, X.W., Ma, X.Y., Deng, Q.D., 1993. Neotectonic activity along the Shanxi Rift system, China. Tectonophysics 219, 305–325.
Yang, J.F., Lu, S.W., Liu, W., Peng, S.M., Zhang, Y.M., 2005. Paleocene Climate and Stratigraphic Era Based on the Sporopollen in Lushi Basin, Henan Province. Gelogical Survey and Research 28, 151–159.
Yin, A., 2010. Cenozoic tectonic evolution of Asia: a preliminary synthesis. Tectonophysics 488, 293–325.
Yue, L.P., Deng, T., Zhang, Y.X., Wang, J.Q., Zhang, R., Yang, L.R., Heller, F., 2004. Magneto stratigraphy of strato-type section of the Baode stage. J. Stratigr. 1, 48–51.
Zhang, Y.P., Huang, W.B., Tang, Y.J., 1978. Cenozoic of the Lantian area. Shaanxi. Science Press, Beijing, pp. 1–64.
Zhang, Y.Q., Liao, C.Z., Shi, W., Hu, B., 2006. Neotectonic evolution of the peripheral zones of the Ordos basin and geodynamic setting. Geol. J. China Univ. 12, 285–297.
Zhang, Y.Q., Ma, Y.S., Yang, N., Shi, W., Dong, S.W., 2003. Cenozoic extensional stress evolution in North China. J. Geodyn. 36, 591–613.
Zhang, Y.Q., Mercier, J.L., Vergdly, P., 1998. Extension in the graben systems around the Ordos (China), and its contribution to the extrusion tectonics of south China with respect to Gobi-Mongolia. Tectonophysics 285, 41–75.
Zhao, W., Hou, G., Hari, K.R., 2016. Two episodes of structural fractures and their stress field modeling in the Ordos Block, northern China. J. Geodynam. 97, 7–21.
Zhou, T.R., Li, H.Z., Liu, Q.S., Li, R.Q., Sun, X.P., 1991. Cenozoic Palaeogeographic Research of Nihewan Basin. Science Press, Beijing pp. 1–162.
Zhu, R.X., Deng, C.L., Pan, Y.X., 2007. Magnetochronology of the fluvio-lacustrine sequences in the Nihewan basin and its implications for early human colonaization of northeast Asia. Quatern. Res. 6, 922–944.